Engineering Structures 342 (2025) 120905

Contents lists available at ScienceDirect

Engineering Structures

journal homepage: www.elsevier.com/locate/engstruct

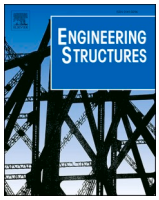

Optimal risk-based design of planar RC frames under progressive collapse: Influence of frame aspect ratio and column cross-section

Lucas da Rosa Ribeiro [a], Felipe Costa Macedo [a], André Teófilo Beck [a], Fulvio Parisi [b,*]

[a] Dept. of Structural Engineering, University of São Paulo, Av. Trabalhador São-carlense, 400, São Carlos, SP 13566-590, Brazil
[b] Dept. of Structures for Engineering and Architecture, University of Naples Federico II, Via Claudio, 21, Naples 80125, Italy

ARTICLE INFO

Keywords:
Frames
Progressive collapse
Reinforced concrete
Risk
Structural optimization
Uncertainties

ABSTRACT

The progressive collapse resistance of reinforced concrete (RC) frame buildings involves complex interactions between structural topology and resisting mechanisms, which strongly influence design for structural robustness. When a RC frame system is subjected to sudden column loss, different complementary resistance mechanisms can be activated in RC beams, depending on beam cross-section detailing and column stiffness. When a double-span beam fails, damage can propagate upwards, affecting upper beams, or laterally, affecting adjacent columns. Both the interaction between resistance mechanisms and optimal design of RC frame depend significantly on the frame aspect ratio and column cross-sections. Taller frames require stronger beams and columns to prevent both vertical and horizontal collapse propagation, whereas lower frames favor weaker beams due to the less critical consequences of upward beam collapse propagation. In this study, the influence of frame aspect ratio and column cross-section on the progressive collapse behavior of planar RC frames is investigated. Analysis results show that the optimal risk-based design of such structures is significantly influenced by the interactions between beam and column moments of inertia, as result of Vierendeel and catenary action intricacies. Specifically, it is shown how the aspect ratio of planar RC frames under multiple ground-floor column loss scenarios leads to different optimal risk-based designs. Nonlinear FE analysis in OpenSees is carried out, capturing Vierendeel, compressive arch and catenary actions in lower, intermediate, and taller RC frames. Weighted Average Simulation is used to compute failure probabilities, and Inverse Distance Weighting is adopted when integrating structural modeling, reliability analysis and risk-based optimization. In contrast to previous investigations, optimal design against progressive collapse is found to mainly depend on balance between beam and column flexural capacities. For the case-study frames, squared cross-section columns lead to greater beam depths, as columns are unable to resist the increased bending moments produced by beams in catenary action. In such cases, ultimate capacity is enhanced by means of compressive arch action. Yet, columns with rectangular cross-sections allow catenary action to be efficiently mobilized in all investigated frames. This later solution closely resembles the 'weak beam – strong column' design philosophy adopted against lateral actions produced by earthquake ground motion and wind.

1. Introduction

Progressive collapse is a cascading failure mode where the loss of a small structural area may lead to widespread and disproportionate damage throughout the structure. Typically triggered by abnormal loads due to extreme events such as fires, earthquakes, floods, and malevolent attacks, progressive collapse is considered as Low Probability/High Consequence (LPHC) event due to its low likelihood of occurrence and extreme consequences. Initial severe damage to either single or a few structural components subjected to abnormal loading can create dynamic load amplification in directly affected parts of the structure, undermining structural integrity in case of limited force redistribution capacity [1–4].

Mitigation strategies depend on the strength of individual members, their interaction capacity, triggering event, and size of initial damage [5–7]. Code-based design approaches typically consider the sudden loss of a supporting element as threat-independent initial damage, highlighting redistribution-type progressive collapse and the role of Alternative Load Paths (ALPs) by means of the Alternative Path Method (APM). In terms of sudden column loss in framed buildings, structural

* Corresponding author.
E-mail addresses: lucasribeiro@usp.br (L.R. Ribeiro), felip_macedo@usp.br (F.C. Macedo), atbeck@sc.usp.br (A.T. Beck), fulvio.parisi@unina.it (F. Parisi).

https://doi.org/10.1016/j.engstruct.2025.120905
Received 27 February 2025; Received in revised form 30 May 2025; Accepted 4 July 2025
Available online 9 July 2025

typology also influences the strengthening strategies as it guides how collapse propagation develops. For instance, slender tall frames primarily experience vertical collapse propagation, whereas wider frames exhibit both vertical and lateral collapse spread [6]. In this regard, Beck et al. [8] demonstrated that the optimal risk-based allocation of strengthening between beams and columns in reinforced concrete (RC) frames depends on the frame's aspect ratio. As beam failures propagate vertically and column crushing (pancake) spreads laterally, lower frames have optimal design margins for beam bending offset by larger margins against column crushing. For lower and wider frames (i.e., small aspect ratio), consequences of beam failure (vertical propagation) are smaller, whereas consequences of column failure (lateral spread) are higher. For taller frames (i.e., larger aspect ratio), failures of both beams and columns tend to be equally severe; hence, risk-based design optimization leads to beams and columns being strengthened simultaneously. Optimal risk-based solutions [8] reveal a competition for a cost-effective allocation of resources to deal with beam failure (vertical propagation) and column crushing (lateral propagation), which strongly depends on the frame's topology.

The investigation in [8] was the starting point for the investigation developed herein. Beck et al. [8] employed the simple analytical model by Masoero et al. [9] to predict progressive collapse response, which could not capture the damaged frame's Vierendeel action, nor the beam's nonlinear post-yielding capacity. Consequently, the optimal risk-based analysis in [8] assumed no complementary resistance mechanisms beyond beam bending and column crushing. While this assumption is reasonable for columns, supplementary mechanisms like compressive arch action (CAA), catenary action (CA), and Vierendeel action (VA) significantly enhance ultimate beam capacity [7,10]. Since these mechanisms depend on substantial axial forces in the beams, the combined axial force and bending moment demands in the columns may exceed those predicted by the analytical model used in [8] until frame collapse occurs.

The analytical model developed by Masoero et al. [9] allows some axial catenary effects to be considered through additional terms in the formulation of ultimate beam capacity. Beck et al. [8] briefly explored those assumptions, demonstrating that catenary effects reduce the likelihood of beam collapse, even with significantly smaller optimal beam design factors. Furthermore, accounting for catenary effects even in the intact frame makes those reduced beam design factors cost-effective for any initial damage probability. Yet, the authors note that this has limited practical relevance, as minimal beam strength would still be required to satisfy serviceability limit states.

In another study, Ribeiro et al. [11] showed that the optimal risk-based design of a fully clamped RC beam leads to an almost squared beam cross-section with increased rebar and stirrup reinforcements, in a progressive collapse situation, and greater beam depth with just enough reinforcements in the intact scenario. Although the optimal beam depth is significantly reduced under greater likelihood of midspan column loss, optimal reliability indices for serviceability failure (i.e., attainment of admissible beam vertical displacement) consistently remained around 3, which was observed to be sufficient to maintain negligible expected cost for this failure mode. In terms of beam bending capacity, the results in [11] agree with those from Beck et al. [8], as a significantly reduced beam moment of inertia is optimal to favor catenary action. As catenary effects are not considered in conventional design (intact frame scenario), beam failure modes related to bending, shear and deflection are more adequate. Hence, results in Ribeiro et al. [11] show that APM strengthening of beams, fully accounting for catenary effects, only becomes cost-effective for local damage probabilities beyond a threshold value, as discussed in Section 3.

In a pioneering study addressing risk-based optimization of RC frames, Ribeiro et al. [12] showed how the optimal frame configurations balance the moments of inertia of beams and columns to prevent premature failure in adjacent columns. When improving column bending capacity is too costly, optimal beam design prioritizes greater depths to enhance its CAA capacity instead of CA, reducing transfer of bending moments to adjacent columns due to VA. Yet, the results in [12] highlighted that columns with rectangular cross-section and greater bending capacity lead to shallower beams with greater CA capacity, which aligns to the optimal solutions in [8] and [11].

Given the impact of beam catenary effects over columns, this study seeks to deepen how the RC frame's aspect ratio influences the optimal risk-based design for structural robustness of a planar RC frame system. Specifically, the investigation examines whether the optimal compromises between beam and column strengths identified in [8] remain valid when accounting for systemic effects of catenary action induced by Vierendeel behavior.

It is known that 3D modeling offers a more complete representation of structural behavior during progressive collapse, particularly due to the contribution of slabs, walls, and other spatial effects. However, this study focuses exclusively on planar RC frames, and this limitation is acknowledged. The primary objective of this work is to understand how progressive collapse influences the optimal configuration of reinforced concrete frames of different aspect ratios. To that end, a 2D approach provides a practical and insightful starting point. Despite its limitations, two-dimensional modeling captures key resisting mechanisms such as flexural action, compressive arch action, and catenary action, all of which are central to progressive collapse mitigation (Section 3.4). While 3D resisting mechanisms can enhance robustness, such as compressive and tensile membrane actions in slabs, they are largely extensions of the mechanisms already captured in 2D. Floor slabs may significantly contribute to the total resistance, but their influence may be considered secondary compared to the primary frame behavior in many typical RC structures with unidirectional slab systems. Yet, to mitigate underestimation, floor slabs and walls are accounted for through their self-weight in the load modeling, and the case studies presented herein are limited to bare RC frames without wall contributions or torsional floor diaphragm effects. Hence, focus is kept on the most influential and fundamental load-carrying members: beams and columns. In addition, the significant influence of central cores is not addressed in this study. Finally, the adopted 2D framework allows the integration of nonlinear structural modeling, reliability analysis, surrogate modeling techniques, and risk-based optimization (each computationally intensive on its own) within a tractable and feasible methodology. This study serves as a rigorous foundation upon which future work will build, including the incorporation of more complex 3D systems.

2. Case-study structures

Five planar RC frames with similar tributary area (number of stories × number of bays) but distinct aspect ratios are investigated, with optimal risk-based design being targeted for lower, intermediate and taller frames (Fig. 1). All configurations have beam spans of 6.00 m, column height of 3.00 m, and columns fully clamped to the ground. For simplicity, all beam spans and columns share identical detailing. Each frame is studied in the intact condition, and in three ground-floor column loss scenarios: exterior column loss (ECL), penultimate column loss (PCL), and middle column loss (MCL). Multiple column loss scenarios are addressed, assuming a single column loss case as initial damage. Some configurations have an even number of columns; in those cases, MCL relates to one of the innermost columns. Besides, non-seismic design conditions are assumed herein.

Unlike [12], this study considers frames extracted from the building's interior, where unidirectional floor slabs impose loads from both sides of the beams. This is done to investigate a worst-case scenario of larger column demands, potentially avoiding the identical optimal column design for both intact and damaged frames that were found and motivated in [12]. Although peripheral columns at the ground floor are more exposed to certain hazards, such as improvised explosive devices (IEDs) and vehicular impacts, it is herein assumed buildings with easy access for vehicles and people at ground floor. Hence, all ground floor

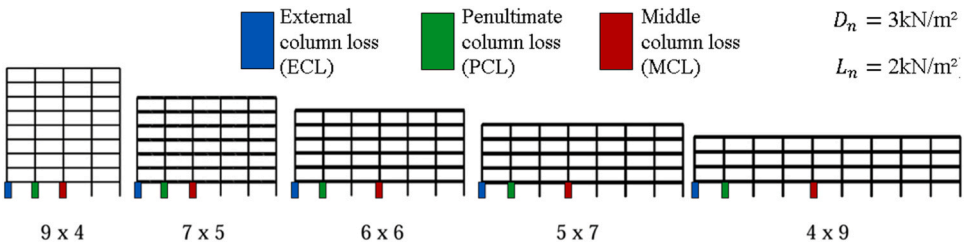

Fig. 1. Studied planar RC frames: column loss scenarios and aspect ratios (stories × bays).

columns within the building become potential targets.

Herein, the consequences of vertical and horizontal collapse propagation are addressed, following [8]: in such analyses, it is essential to simplify the problem by identifying critical failure sequences [13]. In this study, if the double-span beam above the missing column(s) reaches failure, all beam spans above are assumed to fail, as all beams share the same detailing. This assumption represents a worst-case scenario in which upward failure propagation is inevitable, thereby ensuring that the potential extent of collapse is not underestimated. Additionally, since all beams in the frame share identical detailing, the failure of a lower story beam in catenary action strongly suggests that the beam immediately above, subject to similar geometric and material constraints, would also enter catenary action and likely fail under redistributed loads, and so on. Importantly, it is not assumed that all upper beams fail simultaneously once the first double-span beam fails, but rather that an inevitable progression of upward beam failures occurs in this scenario. Hence, the final damaged area due to this sequential upward beam failure is assumed to encompass all beams above the first double-span beam, as shown in Table 1.

If the adjacent columns fail, the damaged area includes the increased beam spans above the total number of failed columns. When the initial set of adjacent columns fails, lateral collapse spread keeps advancing until the increased beam spans reach rebar rupture or shear failure. According to [12], for RC frames with bay length of 6 m, a single stage of adjacent column collapse is observed, as the probability of rebar and shear failure for the increased span exceeds 0.99 (span of 18 m in PCL, and 24 m in MCL).

In this study, the only progressive collapse mitigation strategy is full frame strengthening, achieved by increasing reinforcements, concrete strength, and cross-sectional dimensions. While structural segmentation might be more suitable than APM strengthening for horizontally aligned frames [14,15], segmentation is not addressed herein to enable a direct

Table 1
List of failure modes considered, limit state functions and damaged areas.

Scenario	Failure mode	k	Limit state function	Sketch of damaged area
Intact structure (I)	Large deflection	5	$g_{I,SE}(\boldsymbol{x}) = \delta_{\text{lim}} - \delta(q_I)$	
	Bending (midspan)	30	$g_{I,BM}(\boldsymbol{x}) = M_{RM} - M_M(q_I)$	
	Bending (beam ends)	30	$g_{I,BE}(\boldsymbol{x}) = M_{RE} - M_E(q_I)$	
	Shear failure	60	$g_{I,SH}(\boldsymbol{x}) = V_R - V(q_I)$	
	Column failure	60	$g_{I,COL}(\boldsymbol{x}) = R(N_R, M_R) - S(N_{SI}, M_{SI})$	
Column loss(CL_i)	Rebar rupture	40	$g_{CL_i,SR}(\boldsymbol{x}) = q_{CL_i,SR} - q_{CL}$	
	Shear failure	60	$g_{CL_i,SH}(\boldsymbol{x}) = V_R - V(q_{CL})$	
	Column failure	80	$g_{CL_i,COL}(\boldsymbol{x}) = R(N_R, M_R) - S(N_{SCLi}, M_{SCLi})$	

initial comparison between frame configurations. Moreover, 'strengthening' relates to APM-oriented design of new structures against progressive collapse in further results shown in this study.

Partial frame strengthening has been shown to be more cost-effective in prior studies [8,12,16], aligning with findings from Praxedes and Yuan [17]. The study by these latter researchers indicated that the first floor requires the highest level of strengthening against an inner column loss, followed by the second floor, to achieve optimal robustness. This is primarily due to the critical failure path associated with catenary action in the double-span beam above a lost column. However, they also observed some beam strengthening extending to upper floors, with reinforcements gradually decreasing at higher floor levels.

Bay pushdown analysis of frames partially strengthened on the first two floors reveals a distinct Vierendeel action behavior compared to fully strengthened frames, altering the overall force vs displacement (pushdown) response until rebar rupture. For squared and horizontally aligned frames, these differences are less pronounced, allowing for the use of the same pushdown curves when estimating progressive collapse response for the sake of simplification. However, in taller and slender frames, bending moments in the first non-strengthened columns often exceed those at the ground floor, leading to notable deviations in the overall pushdown behavior. Consequently, full frame strengthening is employed to ensure realistic results for all configurations. Future studies will explore these aspects in greater detail.

3. Methodology

This study investigates the optimal risk-based design of conventional RC frames with varying aspect ratios under gravity loads and column loss scenarios, focusing on how their topologies influence allocation of the strengthening budget between beams and columns, accounting for nonlinear structural behavior of the entire frame. Redistribution-type progressive collapse due to single column loss is analyzed, considering only intrinsic resisting mechanisms. Progressive collapse is mitigated by enhancing ALPs through APM design, following typical codified frameworks. The analysis is limited to primary RC frames supporting unidirectional floor slabs, for which 3D effects can be neglected. Optimization variables of beams and columns include cross-sectional dimensions, concrete strength, and longitudinal and transverse reinforcements.

Under multiple hazards, progressive collapse probability $P[C]$ can be computed as follows [18]:

$$P[C] = \sum_H \sum_{LD} P[C|LD,H]P[LD|H]P[H] \quad (1)$$

where $P[H]$ is the annual probability of hazard occurrence; $P[LD|H]$ is the conditional probability of local damage given H; and $P[C|LD,H]$ is the conditional probability of collapse given LD and H. Although $P[H]$ in Eq. (1) relates to an annual rate of hazard occurrence, herein we address the probability of hazard occurrence over a 50-year period $P[H_{50}]$, corresponding to the typical design lifespan of buildings. This probability is derived from the assumed annual occurrence rate of the hazard $P[H_{50}] = 1 - (1 - P[H])^{50}$.

In order to focus on structural system behavior, given single column loss scenarios, the threat-independent approach proposed by Beck et al. [8,19,20] is used when computing $P[C]$. The authors addressed Eq. (1) by considering the (fifty-year) probability of local damage, $p_{LD} = \sum_H P[LD|H]P[H_{50}]$, as an independent parameter related to epistemic uncertainty in abnormal loading scenarios and local damage occurrence [19]. With this approach, risk analysis can be carried out with no need to estimate $P[LD|H]$ and $P[H]$ (or $P[H_{50}]$), so $P[C]$ is given in terms of optimal system behavior under given values of p_{LD}. Varying p_{LD} from ~0–1 covers situations of negligible to significant column loss threats, revealing how the optimal risk-based solutions adapt to increasing threats [8,21]. Hence, p_{LD} is the main parameter to decide if a specific building should be strengthened against progressive collapse, or not. The local damage probability threshold p_{LD}^{th} represents the break-even point, which makes the additional cost of APM strengthening equal to the reduction in expected cost of progressive collapse failure [8,11,12]. When risk analysis for a specific building shows that $p_{LD} > p_{LD}^{th}$, APM strengthening becomes cost-effective. For a particular building, p_{LD} is estimated in a risk assessment considering building location, surroundings, ownership, use, and all potential hazards and possible local damage scenarios [8,11,12]. Therefore, cost-effectiveness of APM strengthening relies on whether the estimated p_{LD} is below or above p_{LD}^{th}.

As shown by Beck et al. [8] and confirmed herein, the threshold local damage probability p_{LD}^{th} varies significantly with frame aspect ratio, particularly when accounting for Vierendeel and catenary systemic effects. In this work, p_{LD} is varied between $p_{LD}^{\min} = 5 \times 10^{-6}$ to 0.1 (in a lifetime of 50 years), describing scenarios where the threat of local damage is negligible, to very significant threat. Besides, $p_{LD}^{\min}$ relates to the 50-year lifespan equivalent to the "de minimis" annual probability $p = 10^{-7}$ [22].

3.1. General framework

Risk-based optimization is used to find the optimal tradeoff between safety and economy, explicitly accounting for uncertainties (specified in Table 2) and individual consequences of all failure modes [23]. Vector of design variables $\boldsymbol{d}$ includes beam and column cross-section dimensions, concrete strength, and reinforcement ratios, whereas a vector of random variables $\boldsymbol{X}$ encompasses uncertainty in loads, material properties, geometric parameters, and structural model. More specifically, design variables are the beam depth h_B, beam rebar diameter ϕ_B (symmetric bottom and top layers, for simplification), beam stirrup spacing s_t, column size h_C (squared cross-section), diameter of column reinforcement ϕ_C, and frame's concrete strength f_c'. Every design variable in $\boldsymbol{d} = \{h_B, \phi_B, s_t, h_C, \phi_C, f_c'\}$ within a design domain $\mathscr{D}$ represents the mean value of a random variable, so $\boldsymbol{d}$ relates to random design variables.

The framework proposed by Ribeiro et al. [11,12] is used, which relies on integrating risk-based optimization, reliability analysis, nonlinear structural modeling, and pushdown response analysis. In this approach, the balance between construction costs and expected costs of failure is optimized for each p_{LD} via Firefly Algorithm [24]. Probabilities of failure are addressed by Weighted Average Simulation (WASM) [25,26], which is required to later compute the respective expected cost of failure. As a simulation method is used for computing failure probabilities, OpenSees [27] is adopted to conduct nonlinear static pushdown analysis [28] via FEM at sample points created over a sampling domain $\mathscr{S}$ via Latin Hypercube Sampling (LHS) [29–31].

Solving an optimization problem that integrates reliability analysis and nonlinear structural response analysis is computationally expensive via traditional methods, as the millions of sample point estimates render the procedure nearly prohibitive. An efficient approach to address this computational burden is the use of metamodels [11,32] or interpolation [12]. Herein, Inverse Distance Weighting (IDW) [33] is used to interpolate the structural response at any point in $\mathscr{S}$ based on the high-fidelity FEM response at the closest support points. Thus, IDW is also used for computing reliability index to hasten the integration between reliability analysis and risk-based optimization, enabling very fast optimization loops [12].

A sample set is created via LHS across the design domain $\mathscr{D}$. For each design sample point, a previous large random variable sample set with their limit state results are used as basis to compute the probability of occurrence and respective reliability index for all failure modes via WASM. Then, a new sample set is then created via LHS across $\mathscr{D}$ for risk-based optimization purposes (initial set of fireflies in the Firefly Algorithm). The reliability indexes for this last sample points are quickly (and accurately) estimated via IDW interpolation in terms of the support points previously evaluated in reliability analysis.

Table 2
Uncertainty modeling.

Category	RV	Distribution	Mean and $\mathscr{D}$ bounds [ ]	Standard deviation	Coefficient of variation	Reference
Geometry	Beam depth (h_B)	Normal	To be optimized [300, 600] mm	1 mm	-	[41]
	Beam rebar diameter (ϕ_B)	Normal	To be optimized [12, 30] mm	-	0.05	[41]
	Stirrup spacing (s_t)	Normal	To be optimized [10, 30] mm	-	0.05 (assumed)	[12]
	Column size (h_C)	Normal	To be optimized [300, 600] mm	1 mm	-	[41]
	Column rebar diameter (ϕ_C)	Normal	To be optimized [12, 30] mm	-	0.05	[41]
Material	Concrete strength (f_c')	Lognormal	To be optimized [25, 45] MPa	-	0.12	[42,43]
	Rebar yield strength (f_y)	Normal	510 MPa	-	0.05	[42]
	Ultimate steel strain (ϵ_{su})	Normal	0.20	-	0.14	[42,44]
Loads	Dead load (D)	Normal	$1.05D_n$	-	0.10	[45]
	50-year live load (L_{50})	Gumbel	$1.00L_n$	-	0.25	[45]
	Arbitrary point in time live load (L_{apt})	Gamma	$0.25L_n$	-	0.55	[45]
Structural model	Model error (M_E)	Lognormal	1.101	0.187	-	[12]

In terms of Eq. (1), $p_{LD} = \sum_H P[LD|H]P[H_{50}]$ refers to the probability that the initiating local damage (column loss) occurs due to an unspecified hazard within a 50-year design life. Importantly, p_{LD} refers to the initiating member loss, i.e., the column assumed to be removed. The subsequent structural response and potential for further damage propagation to directly or indirectly affected members are captured by $P[C|LD,H]$, which is computed through the proposed framework. While APM relates to a deterministic scenario in which a column is assumed to be suddenly removed, this does not imply that p_{LD} is equal to 1 in a probabilistic context. Instead, the column removal is a modeling assumption used to assess structural robustness under a rare but plausible initiating event for the addressed structure. Herein, this propensity is given in terms of p_{LD}.

3.2. Risk-based optimization

To find the optimal compromise between safety and economy, the total expected cost C_{TE} is minimized for each frame and for each p_{LD}. Herein, C_{TE} addresses manufacturing costs and expected costs associated with all failure modes:

$$C_{TE}(\boldsymbol{X},\boldsymbol{d}) = C_M + \sum_{i=1}^{NIF} k_i C_{MAi} p_{fi} + \sum_{k=1}^{NCL}\sum_{j=1}^{NCLF} k_j C_{MAj} p_{fj} p_{LDk} \quad (2)$$

where C_M is the frame construction cost; *NIF* and *NCLF* are the number of failure modes for intact and damaged structure, respectively; *NCL* is the number of missing column scenarios; k is a subjective failure consequence factor; p_f is the probability of occurrence; C_{MA} is the construction cost of the damaged frame area affected by a given failure mode; and p_{LD} is the local damage probability assumed. Additional life-cycle costs could be included in this objective function, but only those related to construction and expected losses are considered herein. Besides, failure modes are assumed to be uncorrelated with each other.

Following Marchand and Stevens [34], multipliers k address the consequence of a specific failure mode in terms of construction cost C_{MA} for the corresponding damaged area [8,12]. Failure cost multipliers are estimated based on construction costs and collapse costs of the Alfred P. Murrah Federal Building, World Trade Center, and Pentagon. Less severe failure modes, such as serviceability (deflections) or bending failure (yielding onset), are assigned with smaller k values. Conversely, brittle shear and column failures are assigned with larger k values, in comparison to ductile beam failures, as shown in Table 1. These values of k are adequate for risk optimization purposes, consistently leading to adequate optimal reliability indexes based on the severity of failure modes [11,12].

The risk-based optimization problem is formulated as follows:

$$\begin{aligned} &\text{find } \boldsymbol{d}^* \\ &\text{which minimizes } C_{TE}(\boldsymbol{d}) \\ &\text{subject to } \boldsymbol{d} \in \mathscr{D} \end{aligned} \quad (3)$$

Beam design variables are depth h_B, rebar diameter ϕ_B (symmetric layers), and stirrup spacing s_t, whereas column design variables are (square) cross-section size h_C and rebar diameter ϕ_C. Concrete strength f_c' also is a design variable, with the same value being assigned for all beams and columns. To ensure that a unique detailing covers all frames in all scenarios, 3 rebars are chosen for both beam layers and 16 rebars for the columns (Fig. 2). Only lower frames (below 6×6) under Normal Loading Condition (*NLC*) could have smaller amount of column rebar given the lower bounds in $\mathscr{D}$ (300 mm for h_C and 12 mm for ϕ_C, as shown in Table 2).

Firefly algorithm is used to solve the optimization problem, relying on 10 optimization runs for each p_{LD} value, 100 iterations per run, and 40 fireflies. An extensive auxiliary search with 10^4 fireflies is quickly done over $\mathscr{D}$ to improve convergence around global optima, keeping only the 40 brightest fireflies in remaining iterations.

3.3. Limit states and reliability analysis

Table 1 shows the limit state functions, the values of failure consequence factor k, and the extent of final damaged area affected by each failure mode (in red), which are based on [12].

Variables in Table 1 are as follows:

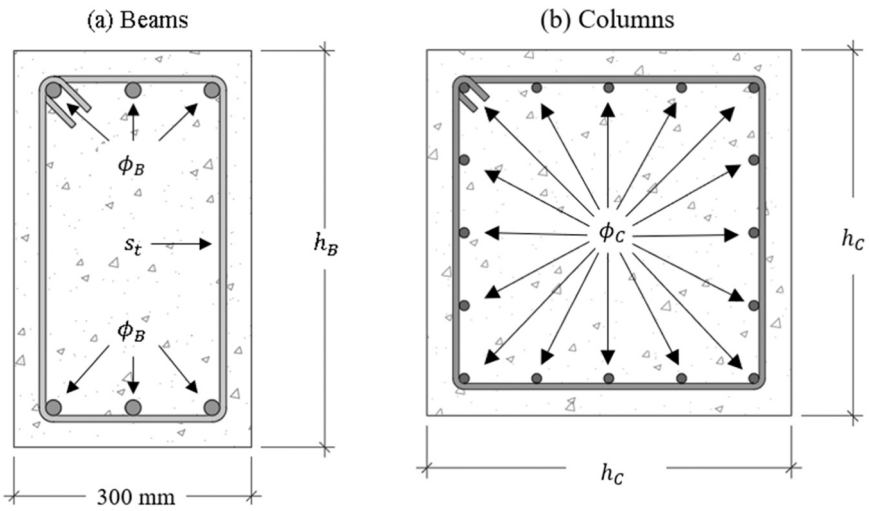

Fig. 2. Adopted cross-section detailing of (a) beams and (b) columns.

- ✓ q_I and q_{CL} are the distributed loads for intact (I) and column loss (CL) scenarios, respectively;
- ✓ δ_{lim} is the admissible beam displacement of 15 mm [35];
- ✓ $\delta(q_I)$ is the beam vertical drift in the intact frame;
- ✓ $M_{RM} = M_{RE} = M_R$ relate to beam bending capacity at midspan (M) and ends (E), respectively [35];
- ✓ $M_M(q_I)$ and $M_E(q_I)$ are the beam bending demands at midspan (M) and ends (E), respectively;
- ✓ V_R is the beam shear capacity [35];
- ✓ $V(q_I)$ and $V(q_{CL})$ are the shear demands in the beams for intact and damaged structure, respectively;
- ✓ $R(N_R, M_R)$ relates to the columns axial force vs bending moment resisting envelope [35];
- ✓ $S(N_{SI}, M_{SI})$ and $S(N_{SCLi}, M_{SCLi})$ are the columns axial force vs bending moment demands for intact and damaged fame, respectively;
- ✓ $q_{CL_i,SR}$ is the beam capacity in terms of top layer rebar rupture at the adjacent beam-column joints.

For column loss scenarios, parameters $q_{CL_i,SR}$, $V(q_{CL})$ and $S(N_{SCLi}, M_{SCLi})$ are obtained in terms of pseudo-static pushdown curve [36–39]. Beam failure modes in the intact frame are considered to happen in a single story, since it is unlikely that live load reaches its 50-year extreme value in all stories simultaneously. Column failure for the intact scenario is checked for at the frame's top corner (greater bending moments) and at the foot of its innermost column (greater axial forces). Hence, the evaluation of column failure in the intact structure scenario is based on two distinct criteria, owing to the symmetry of the planar frame. Specifically: a) in the innermost column located at the first story, both axial force and bending moment demands are checked against their capacity envelope, as those internal forces are significant in that location; b) at the top corner of the frame, only the bending moment is evaluated, since the axial force is negligible in that region, and also to avoid one more structural analysis output in surrogate estimation. Therefore, column failure is deemed to occur if either of these two criteria is not satisfied for a given sample point. This dual-check approach ensures that both critical regions of the column are adequately considered in the reliability evaluation.

For clarity, middle column loss scenario in the squared frame is chosen to depict the damaged areas in Table 1, but the actual damaged frame portion depends on which column is suddenly lost and on the frame topology.

In the column loss scenarios, both rebar rupture and shear failure refer exclusively to failure mechanisms in the beams, not the columns. The red area in the sketch (Table 1) indicates the portion of the structural frame ultimately affected by the assumed failure mode. This includes the area influenced by upward propagation of beam failure. While the structural assessment focuses on the first-story double-span beam directly above the removed column, it is assumed that if this beam fails (by rebar rupture or shear), then the beams directly above are also considered susceptible to failure due to identical detailing. This leads to a worst-case scenario in which the entire vertical bay of beam spans above the removed column is assumed to collapse, thereby also involving the interstory columns between these beams. Besides, as it is unlikely that a value close to the 50-year extreme live load is acting during a hazard even able to trigger column loss, the arbitrary point in time live load is used for the damaged scenarios.

Horizontal failure propagation following adjacent column loss is treated in a simplified yet conservative manner [12]. In reality, the lateral spread of collapse may extend beyond the second spans, depending on complex dynamic effects such as impact forces from falling members, inertial amplification, and system-level interactions (e.g., inward pulling mechanisms typical of domino-type progressive collapse). Nevertheless, these phenomena are not explicitly modeled here, as doing so would fall beyond the scope of this study. Instead, it is assumed that lateral propagation is governed by the residual capacity of individual members and their span lengths.

In the configuration considered, failure is assumed to extend up to the second adjacent spans on each side, beyond which the resulting beam spans are considered too long for the RC beams to sustain redistributed loads without intermediate support (e.g., 12 m for external column loss and 24 m for middle column loss). In the other extreme, assuming a full-structure collapse from lateral propagation would result in unrealistically long, unsupported beam spans, and thus it does not represent a suitable general-case assumption. It is acknowledged that this simplification does not fully capture the complexity of real collapse scenarios. Nonetheless, it offers a practical balance between accuracy and computational feasibility within the adopted optimization-based methodology. Importantly, even under this simplified assumption, further results demonstrate a consistent tendency to avoid lateral progression of collapse following adjacent column failure. As reflected in the optimal solutions, reliability indexes associated with these scenarios are systematically the highest when compared to other failure modes, highlighting their critical influence on structural safety.

Table 2 shows the adopted uncertainty modeling for reliability analysis at the design support points. Based on [11,12], boundary values for $\mathscr{S}$ are chosen in terms of $\boldsymbol{\mu} \pm 2\boldsymbol{\sigma}$ for each random variable. Although this range is not optimal for computing small probabilities via WASM, it is accurate enough for our risk optimization purposes (i.e., probabilities below 10^{-4} relate to negligible expected costs of failure). Therefore, high accuracy for smaller probability values is not necessary.

Table 2 also depicts the boundary values in $\mathscr{D}$ for all random design variables $\boldsymbol{d}$. For those bounds, reasonable values are chosen to ensure compliance with minimal and maximal design requirements related to cross-section dimensions, reinforcement ratios (longitudinal and transversal) and member slenderness [35]. Hence, the chosen design domain leads to all optimal solutions in 4 satisfying these expected guideline requirements. Fixed parameters are as follows: concrete cover of 40 mm; rebar spacing of 100 mm for beams and at least 100 mm for columns; beam stirrup diameter of 8 mm (2 legs); and column transversal detailing consisting of 6-mm stirrups spaced by 150 mm (2 legs).

3.4. Structural analysis

OpenSees is used for structural analysis via FEM. Following Praxedes [40], each span is discretized in 5 fiber displacement-based finite elements, each of them having 3 Gauss-Lobatto integration points). Specifically, 3 elements are used for the member itself and 1 element for each beam-column joint. Co-rotational transformation is used to account for large geometrical nonlinearities, and cross-section layering consists of 200 fibers for confined concrete and 10 fibers for each unconfined concrete cover, which is enough to avoid convergence issues across $\mathscr{S}$. Bay pushdown analysis [28] is performed with a displacement-based integrator, using Krylov-Newton method to solve the nonlinear problem. An initial displacement increment of 1 mm is adopted at the location of the missing column, but an adaptive algorithm is used to enhance or decrease the step depending on the lack of or need for convergence improvement, respectively.

Two load steps are considered in bay pushdown analysis: a) nominal dead and live loads, along with self-weight, are applied to all beam spans; b) if beam rebar rupture does not occur, an increasing load is applied to spans adjacent to the lost column until rupture is verified. Constitutive models for concrete and steel rebars are similar to [12]. The modified Park-Kent model [46] is used to simulate concrete behavior in compression, whereas the tensile behavior is represented according to fib Model Code [47]. All parameters related to concrete modeling are implemented in the 'concretewBeta' model in OpenSees, which effectively captures softening and residual stresses. Rebar behavior is modeled with OpenSees 'ReinforcingSteel' to accurately represent steel behavior and to avoid stress discrepancies that are common in simpler bilinear models.

While it is true that there are some dynamic loading effects on adjacent, indirectly affected bay areas, their influence is comparatively smaller and was therefore neglected in the present study to maintain feasibility within the probabilistic reliability framework. Including all load contributions across the full structures would significantly increase computational demands, especially given the nonlinear simulations, surrogates and reliability analysis employed.

Dynamic effects of sudden column loss can be modeled using explicit dynamic analysis, Dynamic Amplification Factors (DAF), or the Energy Equivalent Method (EEM). As done in [12], EEM is chosen for its practicality, using the pushdown curve and energy conservation principles to build the pseudo-static pushdown curve, which is a reasonable estimate of the dynamic behavior [17].

4. Results

In the following, superscript '$*$' indicates the optimal value of the given design variable. For each frame and column loss scenario, individually, optimal risk-based design is investigated under increasing value of p_{LD}. All costs are related to a single planar frame at a time, not an entire building. Hence, they are naturally smaller in magnitude. Yet, they still reflect meaningful decisions within the optimization framework. Besides, as mentioned in 3, 10 independent optimization runs are conducted at each p_{LD}. However, as a very low dispersion was identified in the results (CoV consistently less than 5 %), only the average results are shown further.

4.1. Optimal design solutions and column loss probability threshold

Fig. 3 shows the evolution of optimal column width h_C^* for p_{LD} ranging from 5×10^{-6} to 10^{-1}. Results for h_B, ϕ_C and f_c' are omitted because identical values are found regardless of p_{LD}, whereas ϕ_B and s_t are omitted because their transition between usual and APM beam design happens at a p_{LD} greater than p_{LD}^{th} (as explained later). For brevity, ECL is chosen to depict Fig. 3, but similar behavior modes are found for PCL and MCL, with differences arising in the total expected costs C_{TE}. Tables and Figures in Appendix A show the optimal results for all frames and columns loss scenarios in greater detail, including optimal beam and column costs per meter.

The yellow background in Fig. 3 corresponds to small p_{LD} values, for which external column loss due to an unspecified hazard is possible but unlikely. The optimal solutions in this region are very similar to the ones which would be obtained in conventional design, under normal loading condition (*NLC*). The blue background corresponds to large p_{LD} values, for which external column loss due to an unspecified hazard is increasingly likely. In this region, optimal risk-based design solutions adapt to mitigate disproportionate collapse. The white background corresponds to local damage probability thresholds [11,12], which change from $p_{LD}^{th} \gtrsim 10^{-3}$ for lower frames, to $p_{LD}^{th} \lesssim 10^{-3}$ for taller frames. The local damage probability threshold p_{LD}^{th} is the break-even point, for which the costs of APM strengthening nearly match the reduction in expected costs of progressive collapse. Such a threshold probability indicates an indifference in the objective function, where two near-optimal solutions coexist: one solution prioritizes alternative load paths with reduced margins for progressive collapse, while the other aligns with conventional design under normal loads. Therefore, two sets of optimal solutions are found, divided by the local damage probability threshold (transition). In the first set (small p_{LD}), optimal solutions favor behavior under *NLC*; in the second set (large p_{LD}) optimal solutions have adapted to mitigate progressive collapse under column loss scenario.

Fig. 3 also shows that C_{TE} at p_{LD}^{th} may reach figures ~2 times greater in comparison to $p_{LD}^{\min}$, especially for lower frames. In such cases, providing progressive collapse mitigation via whole frame strengthening only pays off for larger values of p_{LD} and greater expected costs of failure. This happens because the final damaged area in case of collapse spread is smaller for lower frames, so expected costs of progressive collapse do not grow as fast as in taller configurations. Hence, as progressive collapse consequences are not as severe for lower and wider frames, APM design only pays off under greater threats. In addition, column bending demands due to Vierendeel action are slightly reduced for lower frames. Yet, alternative progressive collapse mitigation strategies could be cost-effective earlier for these lower aspect ratios [12,14], but whole frame strengthening is chosen herein to allow more direct comparisons.

Figs. 4 and 5 show the typical optimal cross sections found for beams and columns, respectively, before and after the threshold p_{LD}^{th}: conventional design for $p_{LD} \leq p_{LD}^{th}$, and APM design for $p_{LD} = 10^{-1}$.

Since inner primary frames receive floor loads from both sides, expected costs of column failure grow faster with p_{LD} in comparison to [12] (as reflected in Fig. 9, to be introduced later). In comparison to primary perimeter frames, mitigating progressive collapse becomes cost-effective earlier for inner frames, especially for taller configurations. Following [8,20], p_{LD}^{th} relates to the first transition between a constant optimal *NLC* design and an APM-oriented optimal design. Hence, optimal APM design for $p_{LD} \gtrsim p_{LD}^{th}$ for squared and taller frames leads to column-only strengthening, to deal with bending demands arising from beam axial forces in both catenary and Vierendeel actions [12]. Horizontal collapse spread is the first propagation mechanism targeted by APM near p_{LD}^{th}, for squared and taller frames, with only h_C showing two transient optimal solutions at p_{LD}^{th}. Upward collapse due to beam failure (rebar rupture or shear) becomes critical for

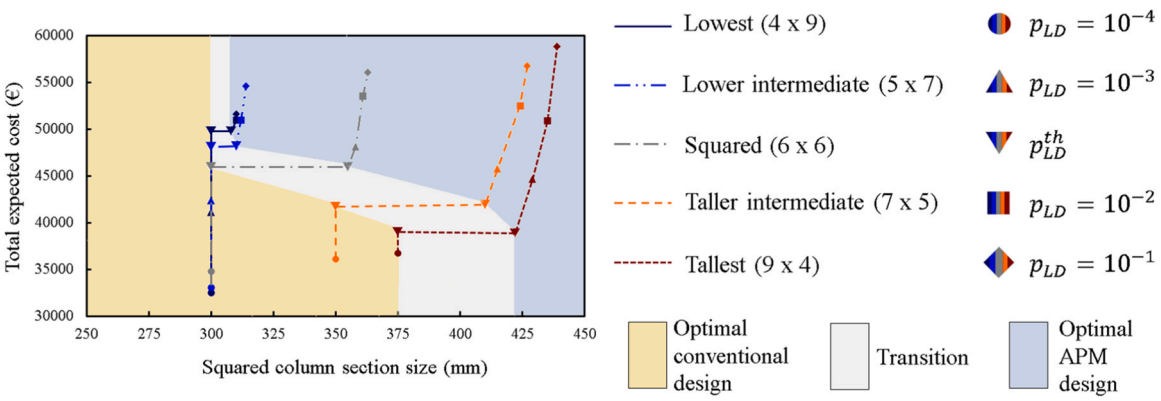

Fig. 3. Optimal results of column width h_C for each frame under ECL as a function of p_{LD}.

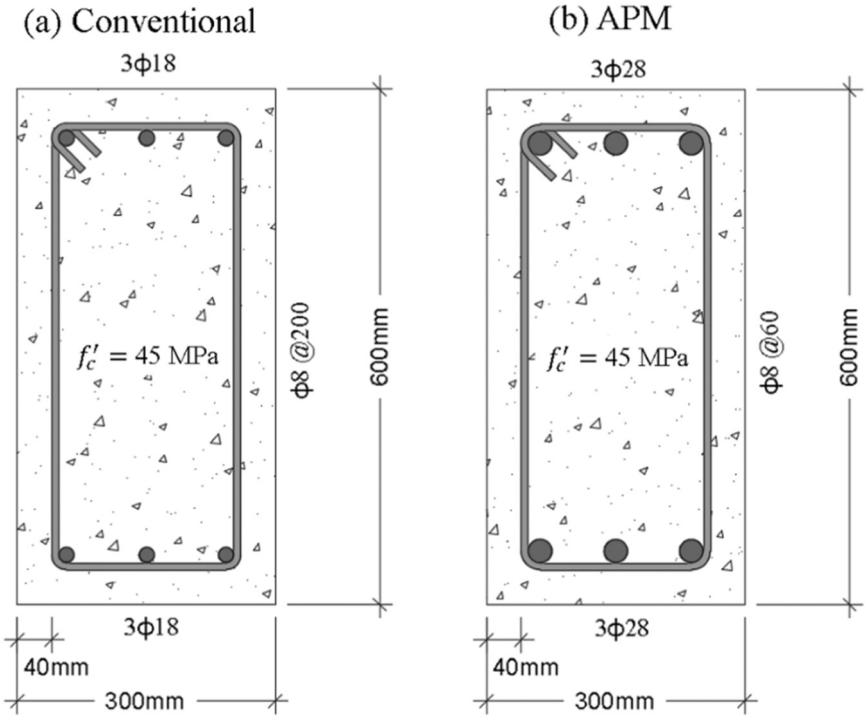

Fig. 4. Optimal beam cross sections for $p_{LD} \leq p_{LD}^{th}$ (a) and for $p_{LD} = 10^{-1} > p_{LD}^{th}$ (b).

$10^{-3} < p_{LD} < 10^{-2}$, where an optimal APM beam design also becomes cost-effective for taller frames (as shown in Fig. 8, to be introduced later). Yet, for $p_{LD}^{th} < p_{LD} < 10^{-2}$, there is an optimal frame detailing given by APM columns and conventional beams for squared and taller frames, and only after $p_{LD} = 10^{-2}$ optimal design solutions become fully APM-oriented.

In addition, overall concrete strength f_c' is shown to be a multipurpose design variable, similarly to h_B. Although it has negligible influence on the pushdown behavior [48], an increased f_c' directly provides greater resistance against 5 failure modes (serviceability, negative and positive beam bending, shear failure and column failure). Therefore, ensuring $f_c'^{*}$ at its upper bound in $\mathscr{D}$ (i.e., 45 MPa) for all frames, scenarios, and regardless of p_{LD}, is the alternative with most cost-effectiveness.

4.2. Optimal resistance and safety margins

Optimal conventional beam design is similar to that discussed in [12]: beam depth up to its upper bound, rebar ratio of 0.42 %, and stirrup ratio of 0.17 %. Load combination $q_I = 1.2DL + 1.6LL$ [35] leads to roughly 64 kN/m over the beam spans, with DL and LL being member loads (kN/m) arising from dead and live loads, respectively. In this framework, Demand-to-Capacity Ratios (DCRs) indicate how the expected (increased) demand matches the expected (reduced) capacity, serving as a normalized and interpretable metric to investigate optimal solutions for intact and damaged structures. Herein, this approach aligns to the Load and Resistance Factor Design (LRFD) for checkup purposes. When computing DL, it is considered the nominal dead load D_n over the floor slabs, and self-weights of the RC beam and slab (depth of 100 mm). Only the nominal live load L_n over the floor slabs is adopted when computing LL.

Hence, DCRs for the intact structure [35] are obtained as follows: 1.03 for bending at the beam ends ($\phi = 0.9$); 0.52 for bending at the midspan ($\phi = 0.9$); and 0.82 for shear failure ($\phi = 0.75$). Since symmetric rebars are adopted, increased safety margin is found for midspan bending. When computing DCR, parameters ϕ relate to strength reduction according to ACI 318–19 [35].

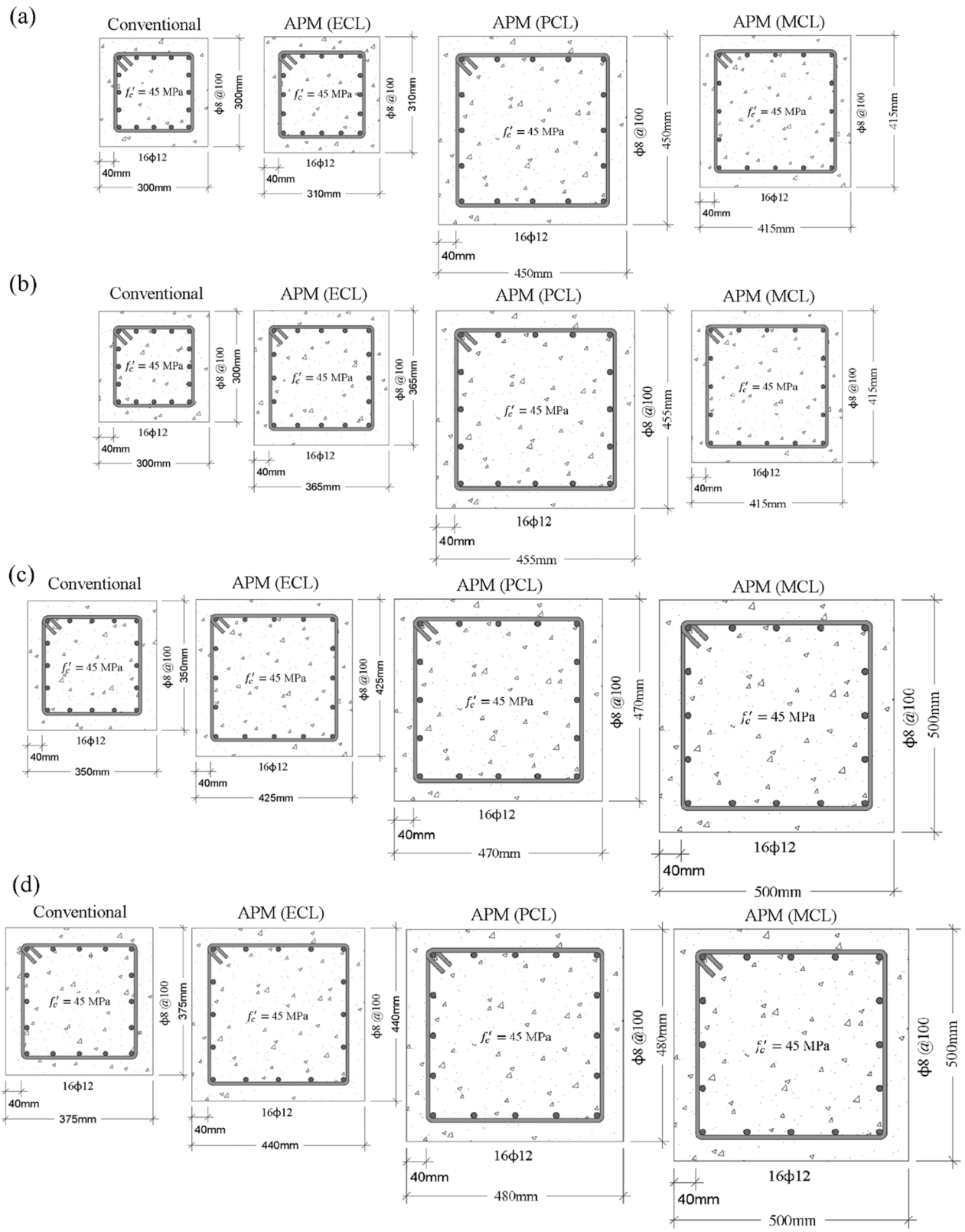

Fig. 5. Optimal column cross sections for $p_{LD} \leq p_{LD}^{th}$ and for $p_{LD} = 10^{-1} > p_{LD}^{th}$: (a) lowest and lower intermediate frames, (b) squared frame, (c) taller intermediate frame, and (d) tallest frame.

In contrast to [12], optimal column designs are not constant with p_{LD}. Besides, optimal conventional column design shows an increased capacity for taller frames, as expected. Combination for usual loading condition $q_I = 1.2DL + 1.6LL$ leads to roughly 64 kN/m in the beam spans (6 m) and ~4.8 kN/m for column spans (3 m). Therefore, the axial force at the base of the inner-most columns is approximately equal to 1550 kN for the lowest frame (4 × 9), 2000 kN for the lower intermediate frame (5 × 7), 2330 kN for the squared frame (6 × 6), 2800 kN for

the taller intermediate frame (7 × 5), and 3600 kN for the tallest frame (9 × 4).

These expected axial demands correspond to 0.36, 0.48, 0.56, 0.52 and 0.59 of the respective optimal axial column capacities, and even an eccentricity of 20 mm still keeps each axial force vs bending demand within the column resisting envelope. The top corner of each frame presents negligible axial forces and bending moments of ~5 % of its greatest axial demand. By comparing these demands with the columns' optimal resisting envelopes, DCRs [35] ranging from 1.2 (taller frame) to 0.77 (lower frame) are obtained. Hence, lower safety margins are allowed for the columns as the frame height increases, reaching DCR > 1 at the top corner ($\phi = 0.9$, mainly flexural demand) and ~0.91 at ground floor ($\phi = 0.65$) for the tallest frame. As the column cost/meter increases for taller frames, avoiding column failure for the intact structure becomes more expensive, especially at the frame's top corner.

Similar to [12], optimal APM beam design is similar for all frames and scenarios, with beam depth equal to 600 mm, maximum concrete strength (45 MPa), rebar ratios up to 1.03 %, and stirrup ratio up to 0.50 %. By addressing DAF = 1.22 (usual value identified in catenary action via pseudo-static pushdown curves), load combination for abnormal loading $q_{CL} = 1.22(1.2DL + 0.5LL)$ [49,50] leads to roughly 64 kN/m over the beam spans. Ultimate load-carrying capacity is found via static pushdown analysis for each frame and each column loss scenario, leading to the DCR factors for rebar rupture shown in Fig. 6 [49, 50]. Since DCR relates to a material property in this case, no strength reduction factor ϕ is used.

Overall DCR factors are ~0.9, indicating a rebar rupture safety margin of ~10 % for all frames over all column loss scenarios (Figure A.1). In terms of reliability index, rebar rupture is related to $\beta^*_{CLi,SR} \approx 3.9$ for all frames in all scenarios, as shown in Fig. 7. Although a previous study for perimeter primary frames have shown $\beta^*_{CLi,SR}$ ranging from 2.32 to 3.20 [12], the greater expected load for an inner frame and imposed use of symmetric beam rebars result in a slightly larger safety margin.

Fig. 6 also reveals a slight decrease in DCR factors for taller frames and scenarios of inner column loss. Larger safety margins for these cases are related to more efficient development of catenary and Vierendeel actions (Figure A.2), so a similar optimal APM beam design is able to attain slightly greater ultimate capacity values. This indirectly explains the reduction in the gap between C_M and C_{TE} for PCL and MCL as the frame height increases (Tables A.2 and A.3 in Appendix A).

When addressing PCL and MCL, lower frames have less stories above the double beam span, and slightly lower axial forces develop during Vierendeel action (Figures A.2 and A.3 in Appendix A). Although the impact on beam capacity is little, it implies a reduced bending demand to the adjacent columns due to the lower number of hanging stories. Thus, the final damaged area is reduced for lower frames in case of lateral collapse spread, as the increased beam span prevents further propagation after failure of a single adjacent column [12]. This results in lower column safety margins (Fig. 7) for configurations with less stories, with $\beta^*_{CLi,CO}$ ranging from 3.0 (lower frame) to 3.5 (square frame), and consequently to greater gaps between C_M and C_{TE} for lower frames (Tables A.2 and A.3 in Appendix A). On the other hand, Fig. 6 reveals that external column loss (ECL) leads to the greatest DCR for rebar rupture. Yet, this relates to the unconditional failure event (disregarding p_{LD}, solely addressing the failure mode itself), as Fig. 7 shows a conditional $\beta^*_{CLi,SR} \approx 4.0$ regardless of aspect ratio. Since catenary action does not develop for ECL (Figure A.2), a reduced size for the squared column section is enough for greater safety margin against horizontal collapse propagation: $\beta^*_{CLi,CO} \approx 4.5$ for smaller frames and $\beta^*_{CLi,CO} \approx 6.0$ for taller frames (Fig. 7 and A.3). Hence, the gap between C_M and C_{TE} is negligible for ECL (Table A.1 in Appendix A).

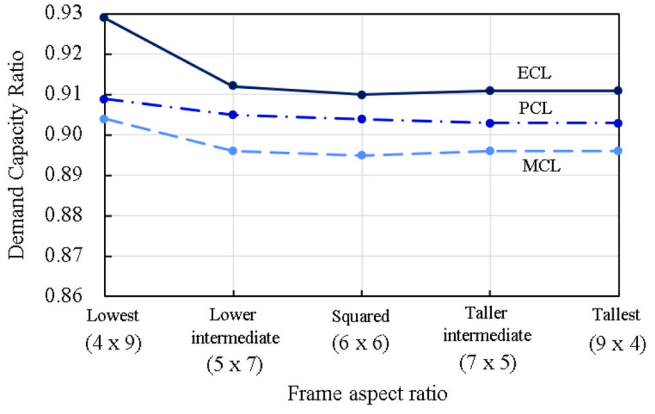

Fig. 6. Rebar rupture DCR factors for APM design ($p_{LD} = 10^{-1}$), as function of frame aspect ratio.

Taller frames have a reduced number of columns, since the tributary area is kept constant, for fair comparisons. Therefore, as the number of remaining columns decreases in column loss scenarios, there is an increase in vertical loads and bending moments to be redistributed to remaining columns, particularly to the adjacent ones. Column bending moments due to Vierendeel action increase for taller frames (Figures A.2 and A.3). This also implies strengthened optimal APM column design solutions, explaining why $\beta^*_{CLi,CO}$ for taller frames increases even for ECL, where catenary action does not develop.

Regarding shear forces, an expected load of 64 kN/m on the affected spans leads to approximately 384 kN of shear at the beam ends. Since the beam has only one vertical support after the column removal, nearly the entire gravity load is transferred to the adjacent beam end by shear. Thus, for a simplified assessment of shear failure DCR, the total distributed load times the entire span length directly corresponds to the shear force at the supported end. Optimal APM beam design leads to DCRs up to ~0.99 (with $\phi = 0.65$), demonstrating that the algorithm ensured a minimal amount of safety margin against shear failure, and Fig. 7 shows $\beta^*_{CLi,SH}$ ranging between 4.0 and 4.6. Symmetric rebars provide greater ultimate load capacity in terms of steel rupture, but without significant increase in shear capacity. Thus, setting beam depth and concrete strength to their upper bounds in $\mathscr{D}$ addresses all failure modes, including shear demands. Yet, stirrup spacing s_t has to be reduced in APM design to produce sufficient shear safety margins. Further reduction in s_t below s_t^* incurs additional strengthening costs that are not compensated by the reduction in expected costs of shear failure.

To characterize the increase in optimal beam resistance, for increasing column loss probability threats (p_{LD}), Fig. 8 shows the optimal resistance factors γ^*, defined in terms of optimal design for $p_{LD}^{\min}$, for bending and shear failure, for each frame and column loss scenario, as in Eq. (4). Hence, γ^* represents the ratio between optimal strength capacity for p_{LD} relative to $p_{LD}^{\min}$:

$$\gamma^*_{CLi,fm} = \frac{R^*_{CLi,fm}(p_{LD})}{R^*_{CLi,fm}(p_{LD}^{\min})} \tag{4}$$

where: *CLi* is the column loss scenario being addressed; and $R^*_{CLi,fm}(p_{LD})$ is the optimal resisting capacity of the failure mode *fm* at *CLi* and p_{LD}.

The overall increase in optimal bending capacity is approximately 2.2 for $p_{LD} \geq 10^{-2}$, while being 1.8 for shear capacity and $p_{LD} > 10^{-2}$. Although lower frames have a smaller damaged area in case of upward collapse propagation, weaker beams are never justified, in contrast to previous results by Beck et al. [8]. In ref. [8], a progressive collapse capacity model that neglects bending moments at adjacent columns shows that stronger beams are only cost-effective for taller frames, where upward collapse propagation is as severe as lateral collapse propagation. Nonetheless, more realistic capacity models reveal that significant axial forces and bending moments in Vierendeel action have

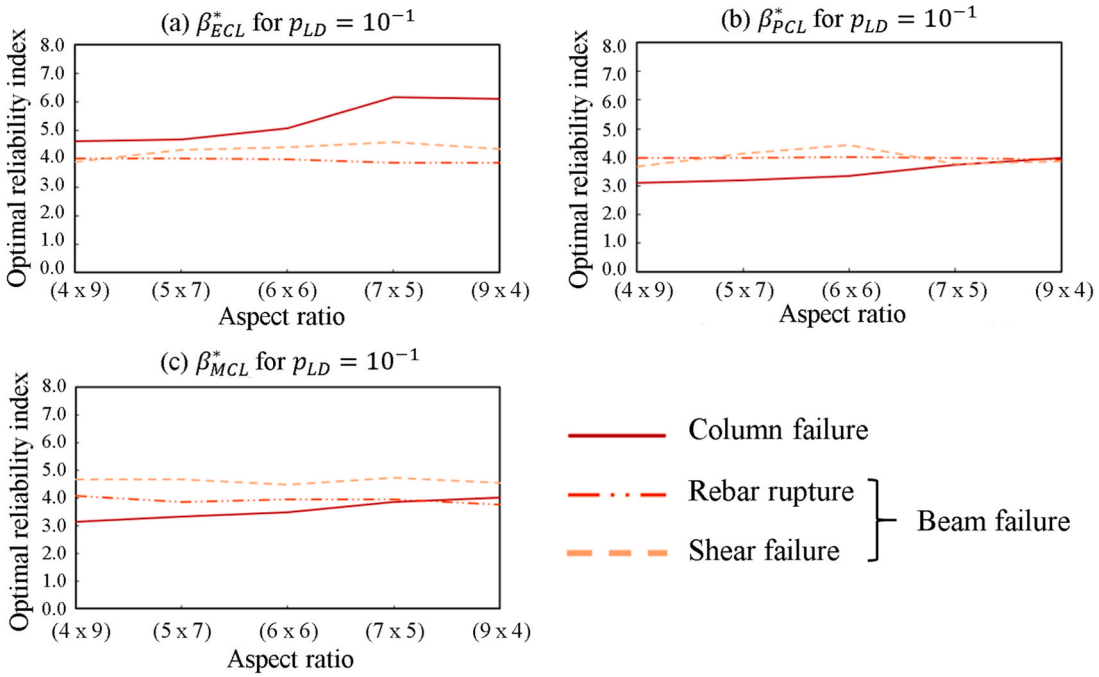

Fig. 7. Optimal reliability indices in terms of frame aspect ratio, for $p_{LD} = 10^{-1}$.

major impacts over adjacent columns.

Weaker beams are able to develop greater ultimate capacity in catenary action [11,12]; however, this also requires earlier onset of catenary action, prematurely increasing bending demands on adjacent columns. For squared-section columns, regardless of frame aspect ratio, enhancing their bending capacity to counteract these demands from catenary action proves cost-ineffective, confirming findings by Ribeiro et al. [12] also for lower and taller frames.

The additional column flexural demand due to tensile forces associated with catenary action increases the likelihood of column failure. In case of column rebar tensile yielding, full achievement of beam ultimate capacity is severely compromised, while column rebar buckling leads to a brittle and sudden column collapse [12]. Nevertheless, an APM beam design with greater depth h_B promotes its ultimate capacity by means of compressive arch action: the onset of catenary action is postponed, reducing the bending demand over the adjacent columns and keeping the expected abnormal loading closer to compressive arch capacity. This motivates the risk-based algorithm's preference for stronger beams independently of the frame's configuration or column loss scenario. Yet, frame ductility prior to collapse is significantly reduced [12].

To address the increase in column resistance, Fig. 9 shows the optimal resistance factors γ^* in terms of axial capacity for each frame and each column loss scenario, as function of p_{LD}. Column axial capacity increases by 90 % for lower frames and 60 % for taller frames, but taller frames still end up with columns of greatest axial capacities. To avoid misinterpretations, the lower frame is used as general reference in the denominator of Eq. (4) (for $p_{LD}^{\min}$). This leads to γ^* greater than 1 (at $p_{LD}^{\min}$) for taller frames, as their column axial capacities are greater than the reference (lower). This allows, in dimensionless terms, the absolute behavior of optimal column axial capacity to be captured.

Although beam APM strengthening becomes cost effective for p_{LD} between 10^{-3} and 10^{-2} (Fig. 8), column APM strengthening turns out to be cost-effective earlier for taller frames (Figs. 3 and 9), even for exterior column loss scenario. Therefore, taller frames have p_{LD}^{th} characterized just by column APM strengthening, reducing the expected cost of column failure caused by greater axial forces and bending moments due to Vierendeel action (Figure A.2).

Fig. 10 shows, for $p_{LD} = 10^{-1}$, how the optimal resistance factors change with the aspect ratio. Optimal APM beam resistance (steel rupture and shear) is found to be insensitive to the frame's aspect ratio and column loss scenario, because stronger beams are required to avoid magnified bending moments being transmitted to the columns, regardless of aspect ratio (Figure A.3). Only column axial capacity is found to be sensitive to frame's aspect ratio, with increasing values being required for taller frames (Fig. 9). Hence, only column results align with those by Beck et al. [8]. Inner column loss scenarios are associated with column-related γ^* factors ranging from 2 (lower frames) to 2.5 (taller frames), while for external column loss such factors range from 1.0 to 1.8, respectively.

4.3. Interpretation of results

This section relates to the case-study frames and assumptions addressed herein. For squared and taller frames, and for $p_{LD} \gtrsim p_{LD}^{th}$, optimal APM design initially strengthens columns to deal with bending demands caused by catenary and Vierendeel actions. Beyond this threshold, optimal design solutions gradually increase beam strength, delineating a fully APM-oriented design for greater p_{LD} values. For lower frames, strengthening the entire structure is cost-effective only under larger p_{LD} and higher expected failure costs. Lower frames experience less severe consequences of progressive collapse due to smaller final damaged areas, reducing the need for extensive mitigation. While Vierendeel action demands are slightly reduced for lower frames, alternative mitigation strategies could become cost-effective earlier for lower aspect ratios, such as segmentation or partial frame reinforcement.

Taller frames show slightly decreased demand-to-capacity ratios under inner column loss scenarios, because both catenary and Vierendeel actions develop more efficiently, enhancing ultimate capacity. Regardless of the frame's aspect ratio, external column loss is the most critical scenario, in terms of DCR. However, conditional reliability indexes for column and beam failures, given ECL, remain consistently above 4 across all frame aspect ratios.

Increased ultimate capacity is ensured for $p_{LD} > p_{LD}^{th}$, with larger longitudinal and transverse reinforcement ratios, and concrete strength at its upper bound. Since columns were assumed with squared cross-

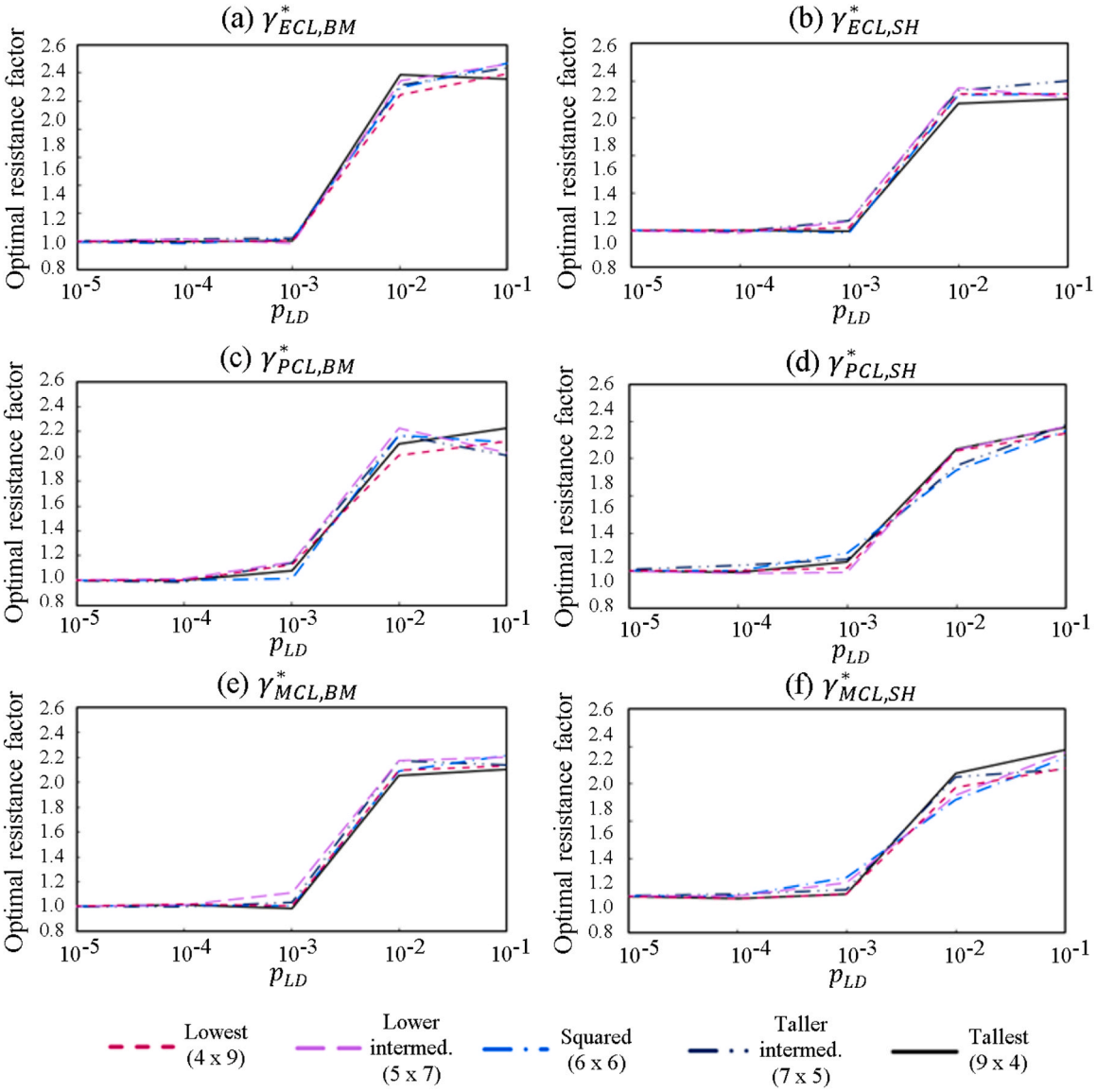

Fig. 8. Behavior of optimal beam γ^* with p_{LD} for each frame and column loss scenario.

sections, it was found to be too expensive to ensure enough flexural capacity to deal with tensile forces that develop under catenary action. Therefore, an optimal beam depth at its upper bound aims at ensuring ultimate capacity by means of compressive arch action. This alleviates the bending demands over adjacent columns and keeps the expected abnormal load closer to compressive arch capacity, while limiting the frame ductility (Figures A.1 to A.3).

Beam cross-section depth and concrete strength are design variables able to ensure capacity against multiple failure modes. Consequently, the risk-based algorithm tends to favor high values for those parameters. Moreover, concrete strength is a design variable with significant uncertainty, so higher values help ensuring sufficient column safety margin in case of non-compliant concrete [51].

ACI provisions [35] for conventional design and both GSA and UFC requirements [49,50] for progressive-collapse-resistant design are met by the optimal solutions found herein, with few exceptions related to DCRs slightly greater than unity. In those few cases, the risk-based algorithm does not show cost-effectiveness in providing greater reinforcements solely to meet safety margins required by the abovementioned guidelines. Yet, slightly more conservative design solutions would be needed to comply with the requirements.

4.4. Remarks on multi-hazard optimal design

International design standards primarily address progressive collapse caused by the sudden loss of a single column [49,50,52], typically triggered by severe (yet often local) events – such as IED detonation or vehicle impact – and propagated through amplified vertical loads. However, progressive collapse can also result from amplified horizontal loads, such as those occurring during seismic events. In such cases, shear forces at the base, excessive node rotations, or extreme inter-story drifts can compromise structural stability and reduce load-bearing capacity [53,54]. Regardless of the triggering mechanism, the propagation of collapse depends on the availability of alternative load paths to redistribute forces and mitigate disproportionate damage [5].

As discussed in [12] and verified by previous results, ultimate beam capacity – defined here by rebar rupture – is directly linked to the flexural capacity of adjacent columns. Resisting mechanisms, such as Vierendeel action, compressive arch action, and catenary action, rely on horizontal restraints provided by the columns. This creates a tradeoff between beam and column moments of inertia: stronger columns with higher moments of inertia enhance ductility and catenary action in weaker beams, while weaker (e.g., squared cross-section) columns

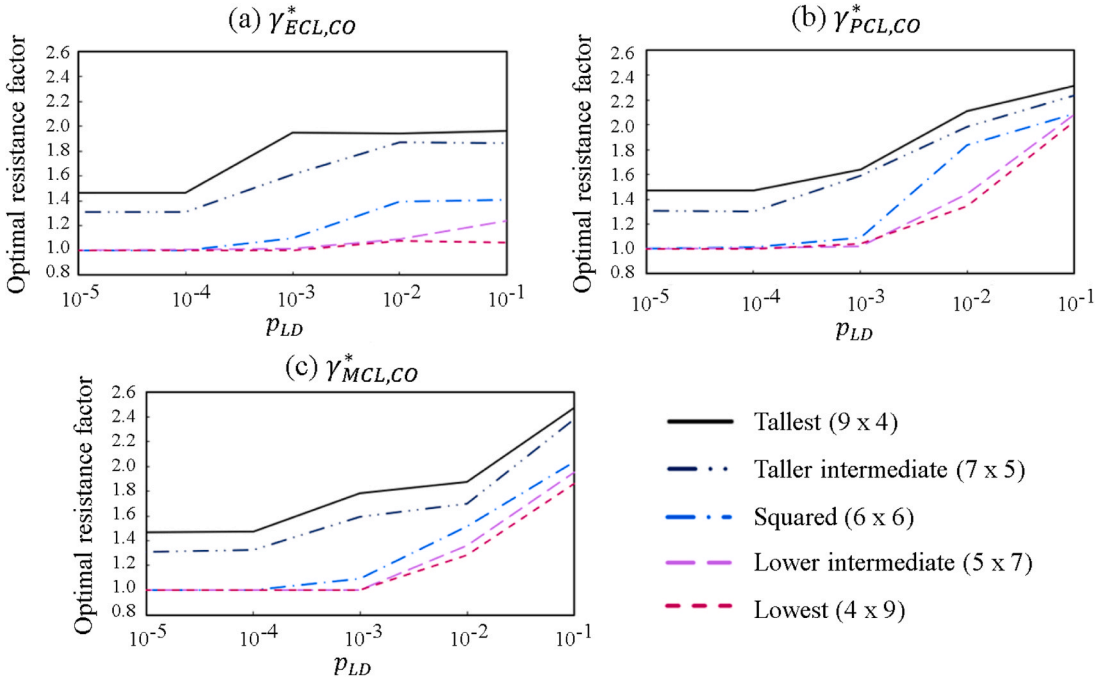

Fig. 9. Behavior of optimal column-related γ^* with p_{LD} for each frame and columns loss scenario.

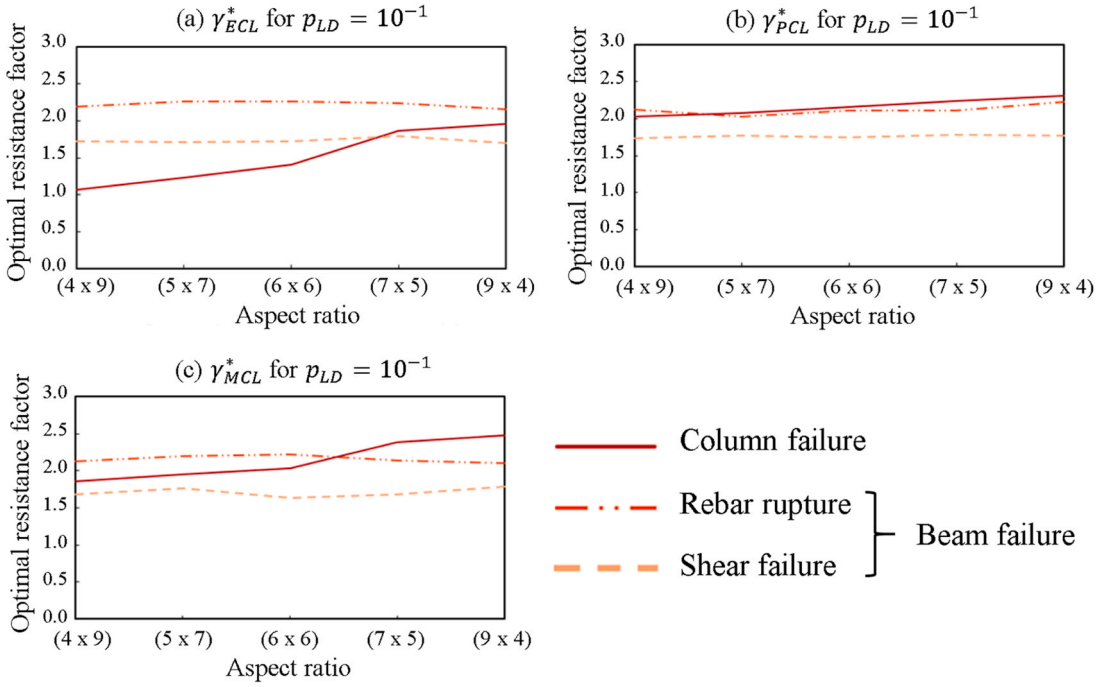

Fig. 10. Behavior of each γ^* with frame aspect ratio.

primarily mobilize compressive arch action in stronger beams but exhibit reduced ductility before collapse. This compromise is found to be significant across a broad range of frame aspect ratios and, contrary to [8], only minor variations are attributable to the frame's topology.

Aligned with results in [12], 'strong column – weak beam' configurations, which are widely used against hazards capable of inducing abnormal lateral loads, such as seismic events, can also optimize progressive collapse resistance for a broad range of frame aspect ratios. Given the increasing frequency of extreme events associated with climate change, such as tornados and flooding, simultaneous optimization for multi-hazard scenarios represents a cost-effective and robust solution [55]. Therefore, results shown in this paper complement those in [12], suggesting optimal configurations which can be cost-effective for progressive collapse mitigation and under abnormal lateral loads, which is particularly relevant for critical infrastructure and taller frames [56]. Optimal designs with weak beams (corresponding to a low moment of inertia) may perform well under multiple hazards during the structure's lifespan, provided that adjacent columns have sufficient flexural capacity. Furthermore, while strong columns with squared cross-sections are not cost-effective for column loss scenarios

alone, they may become viable if the optimization also considers, for instance, significant multi-axial earthquake and tornado actions. These aspects will be further explored in future studies.

5. Conclusions

The optimal risk-based design of 2D reinforced concrete frames vulnerable to progressive collapse depends heavily on the interaction between the moments of inertia of beams and columns. This study explores how the frame's aspect ratio influences optimal designs to mitigate collapse propagation. The findings highlight the importance of balancing strengthening costs against expected costs of progressive collapse across various column loss scenarios for low, intermediate, and tall frames. The results also identify when robust designs using the Alternative Path Method become cost-effective.

Even though the investigation of 3D structural models is more comprehensive than its 2D counterpart, the principles derived from this study can guide practical decision-making, especially during preliminary design. Moreover, the 2D framework allows the integration of detailed nonlinear modeling, reliability analysis and risk-based optimization, which would be significantly more complex for 3D structural systems. Hence, the adopted approach strikes a balance between feasibility and depth of investigation, offering practical insights that are directly transferable to engineering practice.

Firstly, it is emphasized that decisions made prior to optimization can influence the preferred balance between beam and column moments of inertia, such as adopting squared cross-sections for columns – a very common approach in studies on the progressive collapse of reinforced concrete frames [38, 42, 57–70]. For the investigated frames, squared-section columns require deeper beams, as they are less effective at resisting large bending moments when beams experience catenary action, and achieving sufficient moment of inertia for squared cross-sections is too expensive. In contrast, rectangular-section columns can efficiently mobilize catenary action across various scenarios. Thus, similarities are observed between progressive collapse-resistant design and the 'weak beam – strong column' philosophy typically used in seismic design. This alignment suggests that multi-hazard optimization can be achievable through coordinated design strategies.

Results obtained herein indicate that balance between beam and column moments of inertia is crucial, regardless of the frame's aspect ratio (in contrast to [21]), as beam behavior under large displacements directly influences column performance. The use of a nonlinear model that captures the complex interactions among all members in a frame until collapse proves crucial, as simpler models fail to account for the interplay between beams and columns flexural capacities.

This research establishes a foundation for future studies on optimal multi-hazard design, emphasizing its importance particularly for taller frames, where columns play a more critical role and progressive collapse mitigation becomes justifiable for smaller threat probabilities. Furthermore, future developments might incorporate ageing and deterioration phenomena in optimal risk-based design, hence accounting for climate change and lacking/ineffective maintenance during the structure's lifetime.

Authorship statement

The authors hereby confirm that they are the sole liable people responsible for the authorship of this work, and that all material that has been included herein as part of the present paper is either the property (and authorship) of the authors.

CRediT authorship contribution statement

Fulvio Parisi: Validation, Project administration, Investigation, Formal analysis, Writing – review & editing, Supervision, Methodology, Funding acquisition, Conceptualization. **André Teófilo Beck:** Writing – review & editing, Supervision, Methodology, Funding acquisition, Conceptualization, Validation, Project administration, Investigation, Formal analysis. **Felipe Costa Macedo:** Formal analysis. **Lucas da Rosa Ribeiro:** Writing – original draft, Software, Formal analysis, Conceptualization, Visualization, Investigation, Data curation.

Declaration of Competing Interest

I hereby declare that, to the authors' knowledge, no conflicts of interest in terms of either financial or personal relationships undermine the objectivity, credibility and validity of the research findings presented in the manuscript.

Acknowledgements

Funding of this research project by Brazilian agencies CAPES (Brazilian Higher Education Council), CNPq (Brazilian National Council for Research, grants n. 309107/2020–2, 441350/2023–2, and 201218/2024–0), and FAPESP (grants n. 2024/16817–0, 2019/23531–8, 2021/12884–7, and 2024/00102–2) is highly appreciated. Also, this study was developed within FAIL-SAFE project ("near-real-time perFormance Assessment of exIsting buiLdings Subjected to initAl Failure through multi-scalE simulation and structural health monitoring", Grant No. P2022X7N2S_002, CUP N. E53D23003350006), which was funded by European Union through Next-GenerationEU programme - National Recovery and Resilience Plan (PNRR) - Mission 4, Component 2, Investment 1.1, PRIN 2022 programme of the Italian Ministry of University and Research (D.D. 02/02/2022, n.104).

Appendix

Tables A.1 to A.3 present detailed risk-based optimization results for external (ECL), penultimate (PCL) and middle (MCL) column loss at the ground floor of the case-study RC frames. Figures A.1 to A.3 present complementary results, as described in figure captions.

Table A.1
Optimal risk-based design addressing sudden loss of the external ground-floor column (ECL)

Frame ($n_{stor} \times n_{bays}$)	p_{LD}	h_B^* (mm)	ϕ_B^* (mm)	s_t^* (mm)	$f_c'^*$ (MPa)	h_C^* (mm)	ϕ_C^* (mm)	C_{TE}^* (€)	C_M^* (€)	C_{Beam}^* (€ / m)	C_{column}^* (€ / m)
Lower (4 × 9)	$\leq 10^{-3}$	600	18	200	45	300	12	32801.41	32708.88	92.38	106.29
	10^{-2}	585	27	66	45	310	12	50985.57	50794.08	169.93	117.41
	10^{-1}	579	28	74	45	310	12	51456.25	51377.28	172.63	117.41
Lower intermediate (5 × 7)	$\leq 10^{-3}$	600	18	200	45	300	12	32567.64	32154.60	92.38	106.29
	10^{-2}	595	28	62	45	314	12	50975.33	50649.30	178.61	119.51
	10^{-1}	597	28	60	45	314	12	54257.57	54050.10	182.17	119.62

(continued on next page)

Table A.1 (*continued*)

Frame ($n_{stor} \times n_{bays}$)	p_{LD}	h_B^* (mm)	ϕ_B^* (mm)	s_t^* (mm)	$f_c'^*$ (MPa)	h_C^* (mm)	ϕ_C^* (mm)	C_{TE}^* (€)	C_M^* (€)	C_{Beam}^* (€ / m)	C_{column}^* (€ / m)
Square	$\leq 10^{-4}$	600	18	200	45	300	12	33785.22	33346.62	92.38	106.29
(6 × 6)	10^{-2}	590	28	67	45	363	12	53785.37	53534.34	177.15	121.19
	10^{-1}	599	28	60	45	363	13	55997.45	55774.44	182.37	130.02
Taller intermediate	$\leq 10^{-4}$	600	18	200	45	350	12	34375.57	34271.58	92.38	118.03
(7 × 5)	10^{-2}	594	28	67	45	427	13	55978.78	55715.94	177.54	146.29
	10^{-1}	594	27	60	45	427	13	56157.77	55928.04	178.55	146.29
Taller	$\leq 10^{-4}$	600	18	200	45	375	12	36975.76	36714.33	92.38	124.15
(9 × 4)	10^{-2}	598	28	81	45	439	12	56823.73	56517.75	171.50	144.25
	10^{-1}	598	28	69	45	439	13	58787.46	58549.50	177.65	149.46

Table A.2
Optimal risk-based design addressing sudden loss of the penultimate ground-floor column (PCL)

Frame ($n_{stor} \times n_{bays}$)	p_{LD}	h_B^* (mm)	ϕ_B^* (mm)	s_t^* (mm)	$f_c'^*$ (MPa)	h_C^* (mm)	ϕ_C^* (mm)	C_{TE}^* (€)	C_M^* (€)	C_{Beam}^* (€ / m)	C_{column}^* (€ / m)
Lower	$\leq 10^{-3}$	599	18	200	45	300	12	33076.68	32708.88	92.38	106.29
(4 × 9)	10^{-2}	593	28	73	45	354	13	54614.52	53008.80	174.40	127.82
	10^{-1}	590	27	65	45	449	12	64986.27	53919.36	170.01	143.31
Lower intermediate	$\leq 10^{-3}$	600	18	200	45	300	12	32862.40	32154.60	92.38	106.29
(5 × 7)	10^{-2}	595	28	73	45	366	13	53047.75	52355.10	174.59	130.76
	10^{-1}	591	27	63	45	454	13	57234.38	53431.80	171.30	145.49
Square	$\leq 10^{-4}$	600	18	199	45	300	12	33398.56	33346.62	92.38	106.29
(6 × 6)	10^{-2}	595	28	77	45	425	12	54329.12	54184.86	170.98	136.93
	10^{-1}	597	28	69	45	456	12	60276.95	57273.84	175.79	153.20
Taller intermediate	$\leq 10^{-4}$	600	18	200	45	350	12	35508.21	34271.58	92.38	118.03
(7 × 5)	10^{-2}	596	28	78	45	442	12	54354.12	53851.98	171.58	141.43
	10^{-1}	596	28	63	45	470	13	58232.14	57498.00	179.09	157.85
Taller	$\leq 10^{-4}$	600	18	199	45	375	12	36955.13	36714.33	92.38	124.15
(9 × 4)	10^{-2}	596	27	66	45	456	13	57823.92	57732.21	171.01	154.03
	10^{-1}	595	28	67	45	480	13	61239.74	59211.54	173.74	160.62

Table A.3
Optimal risk-based design addressing sudden loss of the middle ground-floor column (MCL)

Frame ($n_{stor} \times n_{bays}$)	p_{LD}	h_B^* (mm)	ϕ_B^* (mm)	s_t^* (mm)	$f_c'^*$ (MPa)	h_C^* (mm)	ϕ_C^* (mm)	C_{TE}^* (€)	C_M^* (€)	C_{Beam}^* (€ / m)	C_{column}^* (€ / m)
Lower	$\leq 10^{-3}$	600	18	200	45	300	12	32808.77	32708.88	92.38	106.29
(4 × 9)	10^{-2}	597	27	79	45	353	15	57923.21	54877.44	172.19	147.37
	10^{-1}	597	28	71	45	421	14	65687.80	56469.84	175.74	154.25
Lower intermediate	$\leq 10^{-3}$	600	18	200	45	300	12	32210.75	32154.60	92.38	106.29
(5 × 7)	10^{-2}	594	28	81	45	403	13	53783.46	52428.60	171.14	137.41
	10^{-1}	600	28	66	45	405	14	60749.27	56522.10	178.69	158.31
Square	$\leq 10^{-4}$	600	18	200	45	300	12	33353.43	33346.62	92.38	106.29
(6 × 6)	10^{-2}	596	27	73	45	394	12	53258.59	52196.04	167.39	127.30
	10^{-1}	594	28	74	45	413	14	60161.73	57777.84	174.04	160.20
Taller intermediate	$\leq 10^{-4}$	600	18	200	45	350	12	34508.48	34271.58	92.38	118.03
(7 × 5)	10^{-2}	584	28	72	45	395	13	54123.66	53933.46	174.02	138.01
	10^{-1}	600	30	87	45	499	12	59779.25	59062.08	180.49	167.93
Taller	$\leq 10^{-4}$	600	18	198	45	375	12	36872.02	36714.33	92.38	124.15
(9 × 4)	10^{-2}	597	27	73	45	426	13	55994.15	55890.54	167.49	146.02
	10^{-1}	596	28	63	45	506	13	62094.55	61569.99	180.09	167.93

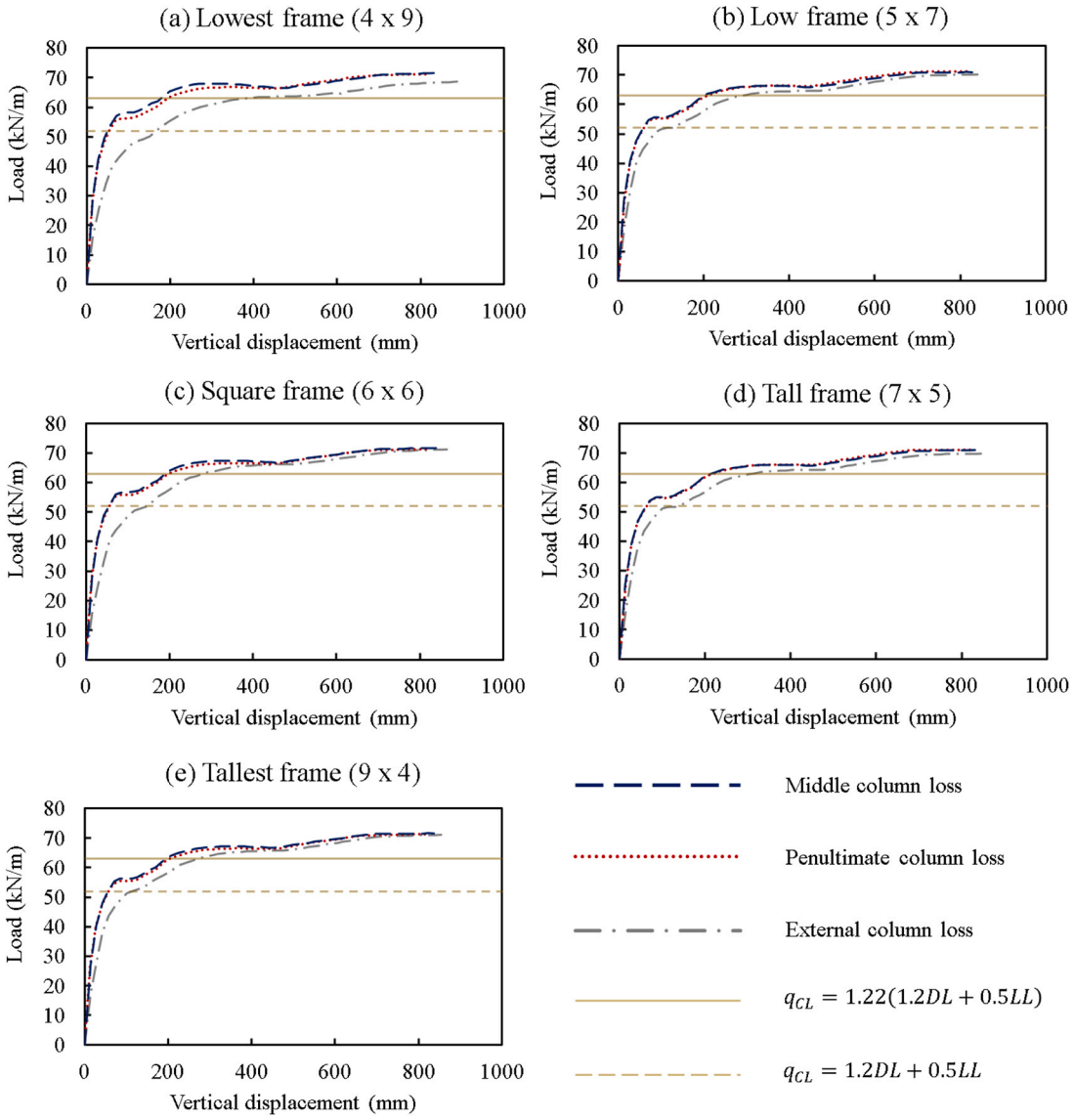

Figure A.1. Bay pushdown behavior of each optimal APM-oriented solution ($p_{LD} = 0.1$) and comparison to expected loads q_{CL} (dynamic effects accounted for when multiplying by 1.22)

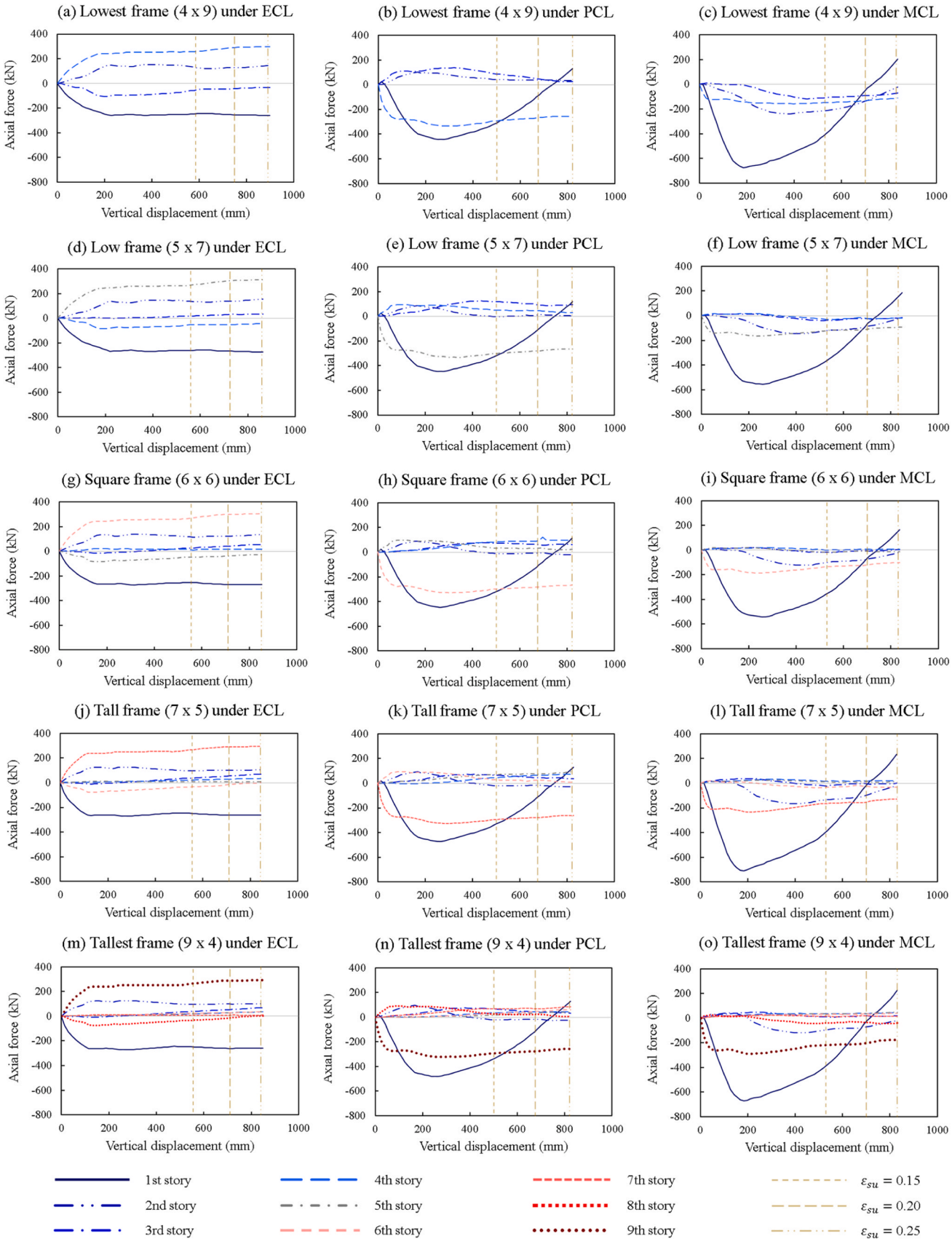

Figure A.2. Axial forces developed in the affected beam spans for the optimal APM-oriented solutions (p_{LD} = 0.1) under each column loss scenario

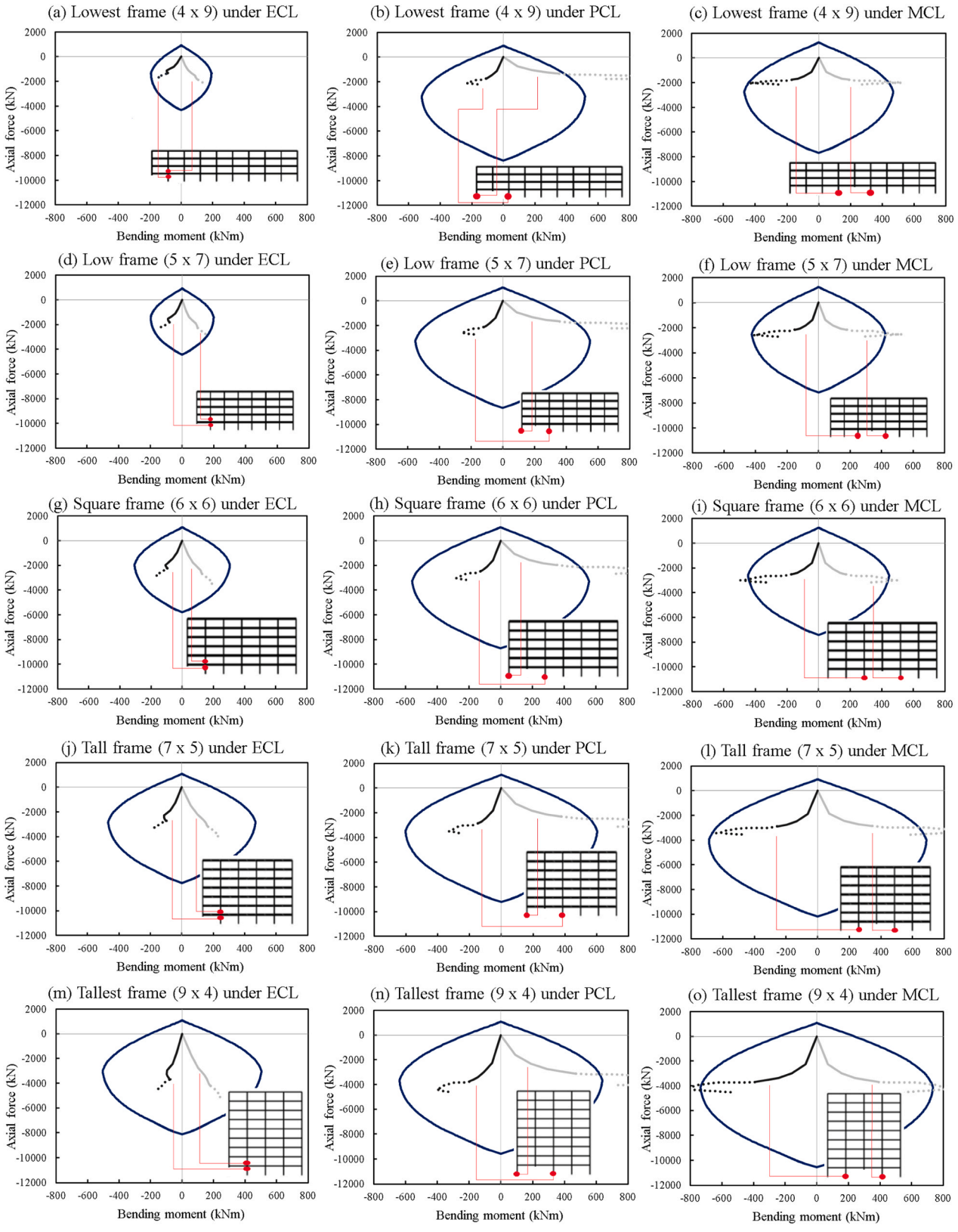

Figure A.3. Demand profiles vs optimal APM-oriented columns resisting envelopes (p_{LD} = 0.1) under each column loss scenario

Data availability

Data will be made available on request.

References

[1] Allen DE, Schriever WR. Progressive collapse, abnormal loads and building codes. Proc ASCE Natl Meet Struct Eng 1972;04. ⟨https://nrc-publications.canada.ca/eng/view/ft/?id=3415baa7-5d26-4dc2-9761-36f882596403⟩. Cleveland, USA, 1972.

[2] Gross JL, Mcguire W. Progressive collapse resistant design (n) J Struct Eng 1983;v. 109(1):1–15. https://doi.org/10.1061/(ASCE)0733-9445(1983)109:1(1).

[3] Parisi F, Augenti N. Influence of seismic design criteria on blast resistance of RC framed buildings: a case study. Eng Struct 2012;v. 44:78–93. https://doi.org/10.1016/j.engstruct.2012.05.046.

[4] Adam JM, Parisi F, Sagaseta J, Lu X. Research and practice on progressive collapse and robustness of building structures in the 21st century. Eng Struct 2018;v. 173:122–49. https://doi.org/10.1016/j.engstruct.2018.06.082.

[5] Kiakojouri F, De Biagi V, Chiaia B, Sheidaii MR. Progressive collapse of framed building structures: Current knowledge and future prospects. Eng Struct 2020;v. 206:110061. https://doi.org/10.1016/j.engstruct.2019.110061.

[6] Kiakojouri F, De Biagi V, Chiaia B, Sheidaii MR. Strengthening and retrofitting techniques to mitigate progressive collapse: A critical review and future research agenda. Eng Struct 2022;v. 262:114274. https://doi.org/10.1016/j.engstruct.2022.114274.

[7] Elkady N, Nelson AL, Weekes L, Makoond N, Buitrago M. Progressive collapse: past, present, future and beyond. Structures 2024;v. 62:106131. https://doi.org/10.1016/j.istruc.2024.106131.

[8] Beck AT, Ribeiro L d R, Valdebenito M, Jensen HA. Risk-based design of regular plane frames subject to damage by abnormal events: a conceptual study (n) J Struct Eng 2022;v. 148(1):04021229. https://doi.org/10.1061/(ASCE)ST.1943-541X.0003196.

[9] Masoero E, Darò P, Chiaia BM. Progressive collapse of 2D framed structures: an analytical model. Eng Struct 2013;v. 54:94–102. https://doi.org/10.1016/j.engstruct.2013.03.053.

[10] Sasani M, Bazan M, Sagiroglu S. Experimental and analytical progressive collapse evaluation of actual reinforced concrete structure (n) Acids Struct J 2007;v. 104(6):731–9. https://doi.org/10.14359/18955.

[11] Ribeiro L d R, Kroetz HM, Parisi F, Beck AT. Optimal risk-based design of reinforced concrete beams against progressive collapse. Eng Struct 2024;v. 300:117158. https://doi.org/10.1016/j.engstruct.2023.117158.

[12] Ribeiro, L. d R.; Rodrigues Da Silva, L.A.; Beck, A.T.; Parisi, F. Risk-based optimization of reinforced concrete frames under progressive collapse. Submitted to Journal of Building Engineering.

[13] Rodrigues Da Silva LA, Torii AJ, Beck AT. System-reliability-based sizing and shape optimization of trusses considering millions of failure sequences. Struct Saf 2024;v. 108:102448. https://doi.org/10.1016/j.strusafe.2024.102448.

[14] Starossek U. Progressive collapse of structures. 2nd ed. ICE Publishing; 2017. https://doi.org/10.1680/pcos.61682.fm.

[15] Makoond N, Setiawan A, Buitrago M, Adam JM. Arresting failure propagation in buildings through collapse isolation (n) Nature 2024;v. 629(8012):592–6. https://doi.org/10.1038/s41586-024-07268-5.

[16] Beck AT, Stewart MG. Risk-based cost-benefit analysis of structural strengthening to mitigate disproportionate collapse of buildings under abnormal blast loading. Structures 2023;v. 57:105103. https://doi.org/10.1016/j.istruc.2023.105103.

[17] Praxedes CSN, Yuan X-X. Robustness-oriented optimal design for reinforced concrete frames considering the large uncertainty of progressive collapse threats. Struct Saf 2022;v. 94:102139. https://doi.org/10.1016/j.strusafe.2021.102139.

[18] Ellingwood BR. Mitigating Risk Form Abnormal Loads and Progressive Collapse. J Perform Constr Facil 2006;20(4):315–23. https://doi.org/10.1061/(ASCE)0887-3828(2006)20:4(315).

[19] Beck AT. Optimal design of hyperstatic redundant structural systems: fundamentals. Eng Struct 2020;v. 219:110542. https://doi.org/10.1016/j.engstruct.2020.110542.

[20] Beck AT, Rodrigues Da Silva LA, Miguel LFF. The latent failure probability: a conceptual basis for robust, reliability-based and risk-based design optimization. Reliab Eng Syst Saf 2023;v. 233:109127. https://doi.org/10.1016/j.ress.2023.109127.

[21] Beck AT, Ribeiro L d R, Valdebenito M. Risk-based cost-benefit analysis of frame structures considering progressive collapse under column removal scenarios. Eng Struct 2020;v. 225:111295. https://doi.org/10.1016/j.engstruct.2020.111295.

[22] Pate-Cornell E. Quantitative safety goals for risk management of industrial facilities (n) Struct Saf 1987;v. 13(3):145–57. https://doi.org/10.1016/0167-4730(94)90023-X.

[23] Beck AT, Gomes WJS. A comparison of deterministic, reliability-based and risk-based structural optimization under uncertainty. Probabilistic Eng Mech 2012;v. 28:18–29. https://doi.org/10.1016/j.probengmech.2011.08.007.

[24] Yang XS. Nature-Inspired Metaheuristic Algorithms. UK: Luniver Press; 2008. ⟨https://www.researchgate.net/publication/235979455_Nature-Inspired_Metaheuristic_Algorithms⟩.

[25] Rashki M, Miri M, Moghaddam MA. A new efficient Simulation method to approximate the probability of failure and most probable point. Struct Saf 2012;v. 39:22–9. https://doi.org/10.1016/j.strusafe.2012.06.003.

[26] Rashki M, Miri M, Moghaddam MA. Closure to "A new efficient simulation method to approximate the probability of failure and most probable point". Struct Saf 2014;v. 46:15–6. https://doi.org/10.1016/j.strusafe.2013.08.002.

[27] Mckenna FT, Scott MH, Fenves GL. Nonlinear finite-element analysis software architecture using object composition (n) J Comput Civ Eng 2010;v. 24(1):95–107. https://doi.org/10.1061/(ASCE)CP.1943-5487.0000002.

[28] Khandelwal K, El-Tawil S. Pushdown resistance as a measure of robustness in progressive collapse analysis. Eng Struct 2011;v. 33:2653–61. https://doi.org/10.1016/j.engstruct.2011.05.013.

[29] Tang B. Orthogonal Array-Based Latin Hypercubes (Taylor & Francis) J Am Stat Assoc 1993;v. 88(424):1392–7. https://doi.org/10.2307/2291282.

[30] Ye KQ. Orthogonal Column Latin Hypercubes and Their Application in Computer Experiments (Taylor & Francis) J Am Stat Assoc 1998;v. 93(444):1430–9. https://doi.org/10.1080/01621459.1998.10473803.

[31] Mckay MD, Beckman RJ, Conover WJ. Comparison of three methods for selecting values of input variables in the analysis of output from a computer code (Taylor & Francis) Technometrics 1979;v. 21(2):239–45. https://doi.org/10.1080/00401706.1979.10489755.

[32] Negrin I, Kripka M, Yepes V. Metamodel-assisted design optimization of robust-to-progressive-collapse RC frame buildings considering the impact of floor slabs, infill walls, and SSI implementation. Eng Struct 2025;v. 325:119487. https://doi.org/10.1016/j.engstruct.2024.119487.

[33] Shepard D. A two-dimensional interpolation function for irregularly-spaced data. In: Proceedings of the 1968 23rd ACM national conference. p. 517-524, 1968. https://doi.org/10.1145/800186.810616.

[34] Marchand KE, Stevens DJ. Progressive collapse criteria and design approaches improvement (n) J Perform Constr Facil 2015;v. 29(5):B4015004. https://doi.org/10.1061/(ASCE)CF.1943-5509.0000706.

[35] American Concrete Institute (Aci). ACI 318-19: Building code requirements for structural concrete. Detroit, Michigan, 2019. 624 p. https://doi.org/10.14359/51716937.

[36] Izzuddin BA, Vlassis AG, Elghazouli AY, Nethercot DA. Progressive collapse of multi-storey buildings due to sudden column loss - Part I: simplified assessment framework (n) Eng Struct 2008;v. 30(5):1308–18. https://doi.org/10.1016/j.engstruct.2007.07.011.

[37] Xu GQ, Ellingwood BR. An energy-based partial pushdown analysis procedure for assessment of disproportionate collapse potential (n) J Constr Steel Res 2011;v. 67(3):547–55. https://doi.org/10.1016/j.jcsr.2010.09.001.

[38] Xue B, Le JL. Simplified energy-based analysis of collapse risk of reinforced concrete buildings. Struct Saf 2016;v. 63:47–58. https://doi.org/10.1016/j.strusafe.2016.07.003.

[39] Bao Y, Main JA, Noh S-Y. Evaluation of structural robustness against column loss: methodology and application to RC frame buildings. J Struct Eng 2017;v. 143(8):04017066. https://doi.org/10.1061/(ASCE)ST.1943-541X.0001795.

[40] Praxedes, C.S.N. Robustness-based optimal progressive collapse design of RC frame structures. Thesis (PhD – Civil Engineering) – Ryerson University, Toronto, Ontario, Canada, 2020.

[41] Joint Committee On Structural Safety (Jcss). Probabilistic Model Code: Part 3: Material properties. 2002. 41 p. Available in: https://www.jcss-lc.org/publications/jcsspmc/ part_iii.pdf. Access in: 14 aug. 2024. https://www.jcss-lc.org/jcss-probabilistic-model-code/.

[42] Parisi F, Scalvenzi M, Brunesi E. Performance limit states for progressive collapse analysis of reinforced concrete framed buildings. Struct Concr Wiley 2019;v. 20:68–84. https://doi.org/10.1002/suco.201800039.

[43] Wisniewski, D.; Cruz, P.J.S.; Henriques, A.A.; Simões, R.A.D. Probabilistic models for mechanical properties of concrete, reinforcing steel and pre-stressing steel. Structure and Infrastructure Engineering, Taylor & Francis, v. 8, n. 2, p. 111–123. https://doi.org/10.1080/15732470903363164.

[44] Galasso C, Maddaloni G, Cosenza E. Uncertainty analysis of flexural overstrength for capacity design of RC beams. J Struct Eng 2014;v. 140(7):04014037. https://doi.org/10.1061/(ASCE)ST.1943-541X.0001024.

[45] Ellingwood B, Galambos TV. Probability-based criteria for structural design (n) Struct Saf 1982;v. 1(1):15–26. https://doi.org/10.1016/0167-4730(82)90012-1.

[46] Park R, Priestley MJN, Gill WD. Ductility of square-confined concrete columns. n. ST4 J Struct Eng 1982;v. 108:929–50. https://doi.org/10.1061/JSDEAG.0005933.

[47] Comité Euro-International Du Béton. CEB-FIP. Model Code 2010: Final Draft. Bulletin D'information, CEB, Lausanne, 2011. https://doi.org/10.35789/fib.BULL.0066.

[48] Yu XH, Lu DG, Qian K, Li B. Uncertainty and sensitivity analysis of reinforced concrete frame structures subjected to column loss (n) J Perform Constr Facil 2017;v. 31(1):04016069. https://doi.org/10.1061/(ASCE)CF.1943-5509.0000930.

[49] General Services Administration (Gsa). General Services Administration Alternate Path Analysis & Design Guidelines for Progressive Collapse Resistance. Washington DC, 2016. https://www.gsa.gov/system/files/Progressive_Collapse_2016.pdf.

[50] Department Of Defense (Dod). Ufc 4-023-03: Desigjn of buildings to resist progressive collapse. Washington, DC, 2009. https://www.wbdg.org/FFC/DOD/UFC/ufc_4_023_03_2009_c4.pdf.

[51] Magalhães FC, Real MV, Da Silva Filho LCP. The problem of non-compliant concrete and its influence on the reliability of reinforced concrete columns. Mater Struct 2016;v. 49:1485–97. https://doi.org/10.1617/s11527-015-0590-x.

[52] European Committee For Standartization, EUROCODE 1: Actions on structures – Part 1-7: General actions — accidental actions. CEN, EN 1991, Brussels, Belgium, 2006. ISBN 9780580837258.

[53] Rodrigues I.D., Cunha J.R.A., Beck A.T. Optimization of a 2D reinforced concrete frame considering a seismic load via cross-entropy method. In: XLIII Ibero-Latin-American Congress on Computational Methods in Engineering, 2022, Foz do

Iguaçú, Brasil. https://publicacoes.softaliza.com.br/cilamce2022/article/view/5380.
[54] Bosse RM, Flórez-López J, Gidrão GMS, Rodrigues ID, Beck AT. Collapse mechanisms and fragility curves based on Lumped Damage Mechanics for RC frames subjected to earthquakes. Eng Struct 2024;v. 311:118115. https://doi.org/10.1016/j.engstruct.2024.118115.
[55] Mattos, L.G.; Carneiro, J.C.C.B.; Beck, A.T. Risk-based optimum design of a device to simultaneously protect building columns against accidental impact, fire and progressive slab collapse. Submitted to Engineering Structures.
[56] Macedo FC, Alminhana F, Miguel LFF, Beck AT. Performance-based reliability assessment of transmission lines under tornado actions. Reliab Eng Syst Saf 2024;v. 252:110475. https://doi.org/10.1016/j.ress.2024.110475.
[57] Yu J, Tan KH. Experimental and numerical investigation on progressive collapse resistance of reinforced concrete beam column sub-assemblies. Eng Struct 2013;v. 55:90–106. https://doi.org/10.1016/j.engstruct.2011.08.040.
[58] Yu J, Tan KH. Structural behavior of RC beam-column subassemblages under a middle column removal scenario (n) J Struct Eng 2013;v. 139(2):233–50. https://doi.org/10.1061/(ASCE)ST.1943-541X.0000658.
[59] Scalvenzi M, Gargiulo S, Freddi F, Parisi F. Impact of seismic retrofitting on progressive collapse resistance of RC frame structures. Eng Fail Anal 2022;v. 131:105840. https://doi.org/10.1016/j.engfailanal.2021.105840.
[60] Weng J, Tan KH, Lee CK. Modeling progressive collapse of 2D reinforced concrete frames subject to column removal scenario. Eng Struct 2017;v. 141:126–43. https://doi.org/10.1016/j.engstruct.2017.03.018.
[61] Sosso B, Andrade SS, Vieira JR, Berke LCM. P. Z. Probabilistic modelling of the robustness of reinforced concrete frames accounting for material property variability using a layered beam finite element approach. Eng Fail Anal 2020;v. 118:104789. https://doi.org/10.1016/j.engfailanal.2020.104789.
[62] Shan L, Petrone F, Kunnath S. Robustness of RC buildings to progressive collapse: influence of building height. Eng Struct 2019;v. 183:690–701. https://doi.org/10.1016/j.engstruct.2019.01.052.
[63] Lew HS, Bao Y, Pujol S, Sozen MA. Experimental study of reinforced concrete assemblies under Column removal scenario (n) Acids Struct J 2014;v. 111(4):881–92. https://doi.org/10.14359/51686739.
[64] Qian K, Li B, Ma J-X. Load-carrying mechanism to resist progressive collapse of RC buildings. J Struct Eng 2015;v. 141(2):04014107. https://doi.org/10.1061/(ASCE)ST.1943-541X.0001046.
[65] Pham XD, Tai KH, Yu J. A simplified approach to assess progressive collapse resistance of reinforced concrete framed structures. Eng Struct 2015;v. 101:45–57. https://doi.org/10.1016/j.engstruct.2015.06.051.
[66] Parisi F, Scalvenzi M. Progressive collapse assessment of gravity-load designed European RC buildings under multi-column loss scenarios. Eng Struct 2020;v. 209:110001. https://doi.org/10.1016/j.engstruct.2019.110001.
[67] Long X, Wang S, Huang X-J, Li C, Kang S-B. Progressive collapse resistance of exterior reinforced concrete frames and simplified method for catenary action. Eng Struct 2021;v. 249:113316. https://doi.org/10.1016/j.engstruct.2021.113316.
[68] Li Y, Lu X, Guan H, Ren P, Qian L. Probability-based progressive collapse-resistant assessment for reinforced concrete frame structures (n) Adv Struct Eng 2016;v. 19(11):1723–35. https://doi.org/10.1177/1369433216649385.
[69] Brunesi E, Parisi F. Progressive collapse fragility models of European reinforced concrete framed buildings based on pushdown analysis. Eng Struct 2017;v. 152:579–96. https://doi.org/10.1016/j.engstruct.2017.09.043.
[70] Zhang Q, Zhao Y-G, Kolozvari K, Xu L. Reliability analysis of reinforced concrete structure against progressive collapse. Reliab Eng Syst Saf 2022;v. 228:108831. https://doi.org/10.1016/j.ress.2022.108831.